

Investigating the role of the Cuvette Centrale in the hydrology of the Congo

PANKYES DATOK¹, Clément Fabre¹, Sabine Sauvage¹, Moukandi N'kaya², Adrien Paris³, Vanessa Dos-Santos¹, Alain Laraque⁴, and José-Miguel Sanchez -Perez¹

¹Université de Toulouse

²Université Marien Ngouabi

³Ocean Next, Grenoble

⁴Institut de Recherche pour le Développement, Toulouse

November 23, 2022

Abstract

15 The increasing pressure on wetland resources continues to threaten the role wetlands play in 16 maintaining the ecological
balance of watersheds. The Cuvette Centrale of the Congo is the 17 greatest intertropical peatland in the world. To fully
understand its role in water resources and 18 ecological services linked to the quality of water and life in the basin, we first
need to quantify 19 its role in the hydrological dynamics. To achieve this aim, we used the Soil and Water 20 Assessment Tool
model (SWAT)-modified for tropical environments-in combination with 21 monthly discharge data. We analyzed water fluxes
entering and flowing out of the Cuvette 22 Centrale of the Congo River Basin on a monthly time scale for the 2000-2012 period.
The 23 model was calibrated, validated, and compared with discharge from gauging stations and 24 surface water elevation
from radar altimetry. Results showed that upland runoff from the 25 Congo River was the highest contributor to the Cuvette
Centrale (33 percent) followed closely 26 by efficient precipitation inside the Cuvette Centrale (31 percent) with right bank
and left bank 27 tributaries contributing 25 percent and 11 percent respectively. We simulated monthly mean 28 interannual
inflows of approximately 34,150 m³ s⁻¹ (88 billion m³) with the main flood peaking 29 in November (45,310 m³ s⁻¹) and total
outflows averaging around 39,860 m³ s⁻¹ (100 billion 30 m³) peaking at 52,430 m³ s⁻¹ in December for the simulation period.
We subsequently estimated 31 a negative monthly mean interannual variation of storage in the Cuvette Centrale wetlands in 32
the order of 5,700 m³ s⁻¹ suggesting that the Cuvette Centrale supplies the river during low 33 water periods. This highlights
the important regulatory function of the Cuvette Centrale and 34 the need for protection of groundwater resources in order to
maintain wetland water quantities 35 and quality. 36

Investigating the role of the Cuvette Centrale in the hydrology of the Congo River Basin

Datok^{1*} P., Fabre¹ C., Sauvage^{1*} S., Moukandi N'kaya² G.D., Paris^{3,4} A., Dos Santos¹ V., Laraque⁵ A., Sánchez Pérez¹ J.M.

(1) Laboratoire Ecologie Fonctionnelle et Environnement, Université de Toulouse, CNRS, INPT, UPS, Toulouse, France.

(2) LMEI/CUSI/ENSP/Université Marien Ngouabi BP 69 Brazzaville Congo

(3) Ocean Next, 90 Chemin du Moulin, 38660, La Terrasse, Grenoble, France.

(4) IRD / CNES / CNRS / UT, UMR5566 LEGOS, OMP, Toulouse, France.

(5) GET-UMR CNRS/IRD/UPS – UMR 5562 du CNRS, UR 234 de l'IRD – 14, av. E. Belin – 31400 Toulouse (France)

Contact : pankyesdatok@gmail.com; sabine.sauvage@univ-tlse3.fr

Keywords: Congo River Basin, Cuvette Centrale, Hydrology, Water balance.

Abstract

The increasing pressure on wetland resources continues to threaten the role wetlands play in maintaining the ecological balance of watersheds. The Cuvette Centrale of the Congo is the greatest intertropical peatland in the world. To fully understand its role in water resources and ecological services linked to the quality of water and life in the basin, we first need to quantify its role in the hydrological dynamics. To achieve this aim, we used the Soil and Water Assessment Tool model (SWAT) – modified for tropical environments- in combination with monthly discharge data. We analyzed water fluxes entering and flowing out of the Cuvette Centrale of the Congo River Basin on a monthly time scale for the 2000-2012 period. The model was calibrated, validated, and compared with discharge from gauging stations and surface water elevation from radar altimetry. Results showed that upland runoff from the Congo River was the highest contributor to the Cuvette Centrale (33 percent) followed closely by efficient precipitation inside the Cuvette Centrale (31 percent) with right bank and left bank tributaries contributing 25 percent and 11 percent respectively. We simulated monthly mean interannual inflows of approximately $34,150 \text{ m}^3 \text{ s}^{-1}$ (88 billion m^3) with the main flood peaking in November ($45,310 \text{ m}^3 \text{ s}^{-1}$) and total outflows averaging around $39,860 \text{ m}^3 \text{ s}^{-1}$ (100 billion m^3) peaking at $52,430 \text{ m}^3 \text{ s}^{-1}$ in December for the simulation period. We subsequently estimated a negative monthly mean interannual variation of storage in the Cuvette Centrale wetlands in the order of $5,700 \text{ m}^3 \text{ s}^{-1}$ suggesting that the Cuvette Centrale supplies the river during low water periods. This highlights the important regulatory function of the Cuvette Centrale and the need for protection of groundwater resources in order to maintain wetland water quantities and quality.

1. INTRODUCTION

Wetlands are an important component of the global ecosystem. It has been pointed out that the wetlands of the world are on a steady decline (Papa et al., 2010; Ramsar Convention on Wetlands, 2018) and this is more worrying considering the ecosystem services they provide (Bwangoy et al., 2013; Davidson, 2014; Keddy et al., 2009; Sauvage et al., 2018). Alluvial wetlands control several physical, chemical, and biological processes (Borges et al., 2015; Bouillon et al., 2014). They can be connected to the river and influence water, sediment and nutrient balances by playing a role in the hydrological dynamics (Weng et al., 2003), in carbon sources or sinks (Peyrard et al., 2008) or in nitrate removal by denitrification (Bernard-Jannin et al., 2017; Fabre et al., 2020; Guilhen et al., 2020; Jung et al., 2010; Kim et al., 2017; Papa et al., 2010; Sun et al., 2016). Fluctuations in wetland water volumes are very important in

48 estimating hydrological and biogeochemical functioning of wetlands as the timing and duration
49 of flood pulses affect fauna and flora, which depend on them directly (Forsberg et al., 1993).

50 After the Amazon basin, the Congo River Basin (CRB) contains the second-largest continuous
51 rainforest on the planet with a covering of 1.8 million km² (Haensler et al., 2013). At the heart
52 of the basin is the “Cuvette Centrale”, a vast forested wetland depression occupying close to
53 half of the watershed with a strong influence over the hydrology and the biogeochemical
54 characteristics of the rivers that cross it (Laraque et al., 1998a, 2009). Alsdorf et al. (2016)
55 summarized the hydrologic studies carried out over the wetland areas of the basin, noting the
56 challenges associated with hydrologic measurements in this part of the CRB. These challenges
57 are a result of the peculiar characteristics which include ill-defined shorelines and the dense
58 forest canopy, which obscure most of the inundated areas. Nevertheless, different approaches
59 have continued to be used to study the wetlands of the (CRB). Traditional or direct methods of
60 hydrological measurements in the Congo basin wetlands are difficult. This is due mostly to the
61 largely ungauged nature of the catchment, the briefness, inconsistency, and unreliability of
62 observable data where they exist, and the accessibility limitations of the physical environment
63 (Munzimi et al., 2017; Runge, 2007; Alsdorf et al., 2016). For these reasons, and to better
64 understand the wetland hydrology, it has become imperative to seek alternative indirect means
65 of measurement. One of these alternative solutions is to combine modeling approaches with
66 the use of satellite remote sensing techniques, which have largely become the only options for
67 in situ data in remote areas (Papa et al., 2010).

68 Altimeters have been recognized as a special tool for measurement of hydrological dynamics
69 in data-scarce regions, with the major drawbacks being its spatial resolution. This is because
70 altimeters are mostly limited by their repeat cycles causing virtual stations to be located far
71 apart (Kugler et al., 2019; Rosenqvist & Birkett, 2002). Kim et al. (2017) generated multi-
72 temporal water level maps over parts of the Congo main-stem based on the relationship
73 between the Environmental Satellite (ENVISAT) altimetry-derived river level changes, the
74 Phased Array type L-band Synthetic Aperture Radar (PALSAR) and Scanning Interferometric
75 Synthetic Aperture Radar (ScanSAR) backscattering coefficient changes. They were able to
76 classify the CRB into permanent open water, forest, macrophytes, and herbaceous plants.
77 Tourian et al. (2016) employed a method using a multi-satellite approach over the Po river (the
78 largest river in Italy), by which all virtual stations of several satellite altimetry missions were
79 connected hydraulically and statistically. This enabled them to densify water level time series
80 at any given location along the river, thus dealing with problems related to the spatial resolution
81 of altimeters. They validated the transferability of their methodology in the CRB. Their
82 densified time series correlated well with Insitu data in the Congo, Mississippi, and the Danube
83 rivers. Yuan et al. (2017) applied the Interferometric Synthetic Aperture Radar (InSAR) and
84 ENVISAT altimetry to generate long term water storage time series over the floodplains of the
85 CRB for the period 2002-2011. They calculated a difference in water volume storage of
86 approximately 4 km³ between wet and dry years of 2002 and 2005, respectively. They
87 concluded that their floodplain water storages were in overall agreement with the seasonal
88 variations of Total Water Storage (TWS) and precipitation.

89 Kim et al. (2019) experimented with a machine learning technique to estimate discharge using
90 stage heights from the Envisat altimetry data obtained from 2002 to 2010. By using a
91 combination of several rating curves established at different points over the CRB, they were
92 able to produce better discharge estimates. Although this process still depends on in situ data,
93 it holds promise for filling in missing data. Combining the Global Inundation Extent from
94 Multi-Satellites (GIEMS) dataset, (Prigent et al., 2007) with ENVISAT altimetry water level
95 measurements, Becker et al. (2018) were able to estimate surface water extent of floodplains,

96 lakes, rivers, and wetlands of the CRB. They found the annual variation in surface water storage
97 in the CRB to be around 80 km³ or approximately 6 percent of annual water volume that the
98 Congo River exports to the Atlantic Ocean.

99 Hydrological models have been deployed with varying degrees of success in the CRB.
100 Modeling in this basin poses several challenges due to the sheer size and heterogeneity of the
101 watershed, as well as the attenuation effects of the Cuvette Centrale (Alsdorf et al., 2016).
102 Chishugi and Alemaw (2009) parameterized the Hybrid Atmospheric and Terrestrial Water
103 Balance model for purposes of computing water resource availability. They simulated soil
104 moisture and runoff of the basin and were able to distinguish two main climatic regions based
105 on the Evapotranspiration ratio. They did this even though their model was not calibrated but
106 only parameterized using global datasets. Tshimanga et al. (2011) calibrated the Pitman-GW
107 model, a conceptual semi-distributed hydrological model, reproducing observed hydrological
108 responses adequately. Significant variations in model parameters were put down to the complex
109 nature of the basin or inadequate model structure. The complexity in hydrological processes in
110 parts of the basin questions the representativeness of these model parameters to the
111 hydrological response. Similarly, Tshimanga & Hughes (2014) used the semi-distributed
112 Pitman model to determine key hydrological processes within the basin and found that it
113 captured the magnitude of high and low flows in the majority of the subbasins within the
114 catchment. The model was not able to satisfactorily capture the runoff response of the central
115 basin and flows downstream of lakes and wetland areas, thereby highlighting the importance
116 of groundwater and channel routing parameters. Recently, Paris et al. (this volume) used a
117 combination of remote sensing datasets and hydrologic-hydrodynamic modeling at the basin
118 scale and on a daily basis to infer hydrologic state all over the basin in near-real-time.

119 Beighley et al. (2011) calibrated the hillslope river routing model in a bid to test the impact of
120 satellite-derived precipitation datasets on streamflow. Three precipitation datasets were tested:
121 The Tropical Rainfall Monitoring Mission (TRMM), the Climate Prediction Centre Morphing
122 Technique Product (CMORPH), and the Precipitation Estimation from Remotely Sensed
123 Information using Artificial Neural Networks (PERSIAN). They found that four parameters:
124 maximum soil moisture deficit, horizontal subsurface conductivity, hillslope surface
125 roughness, and channel roughness were the most sensitive. The tests showed that the TRMM
126 estimates agree more with historical data compared to CMORPH and PERSIAN as it matched
127 observed data more closely. They also showed that satellite rainfall showed discrepancies in
128 equatorial regions of the basin. Others analyzed climate change scenarios in the CRB with
129 different predictions for hydrologic variables (Alloysius et al., 2016; Tshimanga and Hughes,
130 2012).

131 The Commission Internationale du Bassin Congo – Oubangui - Sangha (CICOS) published in
132 2016 a report (BRLi, 2016), which included water balance studies of the CRB. Using the
133 hydrological model Mike Hydro Basin (MHB), they estimated -an average variation in storage
134 in the Cuvette Centrale of approximately 1.3 billion m³ of water for the period 1951-2012.
135 More recently, Munzimi et al. (2019), using the Geospatial Streamflow Model (GeoSFM)
136 semi-distributed hydrological model, achieved acceptable modeling by applying a basin and
137 subbasin “ensemble calibration” approach with a selection of appropriate model routines and
138 parameters to slow the flow of water across the basin. They were also able to capture the flow,
139 seasonality and timing at all locations calibrated with their model.

140 It is evident that within the last two decades, there have been remarkable advances in the
141 approaches used to study the hydrology of the CRB. However, it is also clear that there remains
142 a lot to be done to fully comprehend the hydrological functioning of the ungauged central

143 portion of the Congo basin. By reason of its location in both hemispheres, the Congo basin
144 experiences two periods of high water and two periods of low water. The two floods are the
145 greater September-October-November (SON) floods influenced by the southern tributaries and
146 a lesser one in March-April-May (MAM) controlled by the equatorial regions. Two low water
147 levels then punctuate these two floods, one in February-March, corresponding to the dry season
148 of the northern part and the other in July-August at the time of the southern dry season. The
149 Cuvette Centrale is uniquely positioned to receive flow from the different tributaries that cross
150 this great basin at different times of the hydrological year. Most of the modeling studies did
151 not consider the spatio-temporal variations in the tributaries that contribute to the Cuvette
152 Centrale and provide little to no distinction on the Cuvette Centrale hydrology based on
153 timescale and seasons. We build on an approach initiated by the BRLi and complementary
154 work done by Moukandi N'kaya et al. (this volume), to estimate the change in storage of the
155 Central Basin, by the first upstream-downstream hydrological balance obtained from
156 calibration and validation of in situ data. Using a mass balance approach, we estimated the
157 fluxes of water feeding into the Cuvette Centrale from eleven tributaries located both on the
158 right and left banks of the Congo River and on the outer fringes of the wetland before they
159 become fully influenced by the wetlands. Afterward, we compared these fluxes with the
160 measured output at the basin outlet in Brazzaville/Kinshasa in order to observe the impact of
161 the Cuvette Centrale on these flows. Knowing the importance of evapotranspiration using this
162 approach, we use a modified Soil and Water Assessment Tool (SWAT) model fitted with a
163 module to better estimate the amounts of water that are removed from the Cuvette Centrale.
164 This will also aid in identifying the source of Cuvette Centrale waters in line with the theories
165 proposed by Alsdorf et al. (2016) concerning the source and emptying of Cuvette Centrale
166 waters. Therefore, the main objective is to enhance our knowledge of the hydrological
167 functioning of the Cuvette Centrale and the limitations of using a distributed hydrological
168 model.

169 Specifically, we intend to:

- 170 (i) Simulate and assess water flows entering the Cuvette Centrale using modeling tools.
- 171 (ii) Analyze the impacts of the Cuvette Centrale on streamflow and the water balance
172 components in the catchment at the basin outlet.

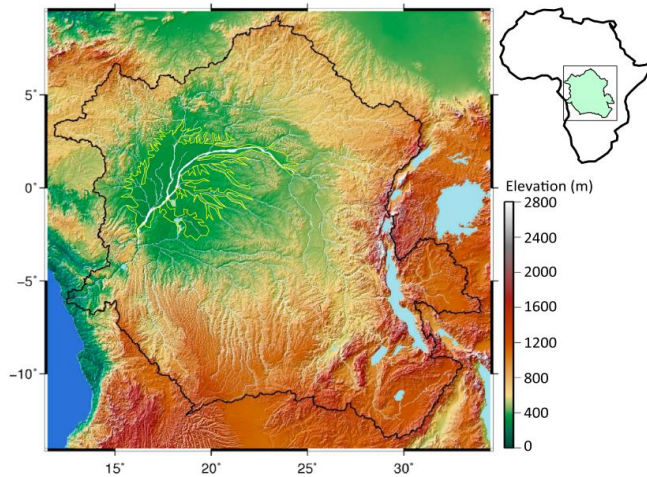
173 These objectives will be met by combining modeling, gauging station data, and satellite data
174 observations in order to represent the hydrological system within the Cuvette Centrale
175 adequately.

176 **2. MATERIALS AND METHODS**

177 **2.1. Study site**

178 In Africa, the Congo River is the second longest river after the Nile at 4,700 km, and first in
179 terms of discharge and basin size - $40,500 \text{ m}^3 \text{ s}^{-1}$ and $3.7 \times 10^6 \text{ km}^2$ respectively - second only
180 to the Amazon globally. The Congo River forms a broad curve that crosses the equator twice.
181 Its basin extends between the parallels 9°N and 14°S and the meridians 11°E and 34°E , with
182 its form, relief, geology, climate, as well as its vegetal cover, structured concentrically around
183 the Cuvette Centrale; - a central depression already described by Laraque et al. (2009, 2013b)
184 (Figure 1). The twin stations of Brazzaville/Kinshasa controls 98 percent of its total area. The
185 Brazzaville/Kinshasa gauge station (Figure 2a) is located approximately 400 km upstream to
186 its oceanic outlet, and the hydrologic input along this last reach is close to $1,000 \text{ m}^3 \text{ s}^{-1}$. The
187 Cuvette Centrale lies at the heart of this basin (see Figure 2b) within longitudes 16° to 20° E

188 and latitudes 2°30' N to 2° S (Davies & Gasse, 1987). It is a vast Cenozoic depression consisting
 189 of clayey and sandy fluvial quaternary alluvial deposits measuring 700 km from North to South
 190 (Laraque et al., 1998a). In periods of high water, the Cuvette Centrale extends from Ouesso on
 191 the Sangha River to Impfondo on the Ubangi River on its right bank (Figure 2a). The Likouala
 192 aux Herbes is the emblematic flooded basin of the Cuvette Centrale during high flow (Laraque
 193 et al., 1998a, 1998b). It also comprises the central portions of the basin, including the Tumba-
 194 Ngiri and Mai Ndombe wetlands and lakes on its left bank, the areas of which are 65,695 km²
 195 (O'Loughlin, 2013).

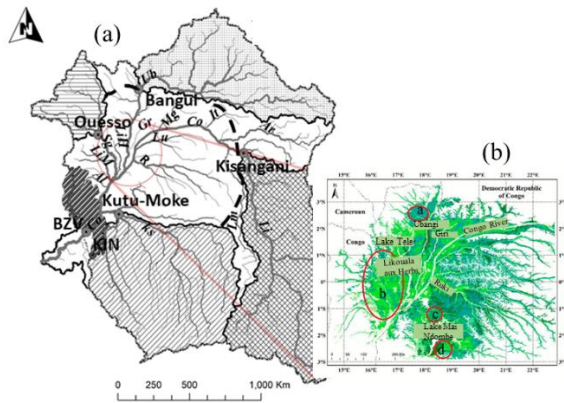


196

197 **Figure 1.** Shuttle radar topography mission (SRTM) digital elevation model (Farr et al., 2007)
 198 of the topography of the Congo River basin showing the area of the Cuvette Centrale within
 199 the yellow polygon as generalized by Bwangoy et al. (2010) (adapted from Alsdorf et al.,
 200 2016).

201

202 The physiography, climate, and vegetation of the CRB are generally centered and extend
 203 around the Cuvette Centrale. The Cuvette Centrale has an equatorial climate with mean rainfall
 204 between 1,800 mm yr⁻¹ and 2,200 mm yr⁻¹ falling throughout the year (Bultot, 1971). The mean
 205 annual temperatures are 25° C (Bernard, 1945) with evapotranspiration at 1,050 mm yr⁻¹
 206 (Bultot, 1971). Bwangoy et al. (2010) using remote sensing delineated an area of 360,000 km²
 207 as the maximum inundated area of wetlands within 5°N to 6° S and 13°E to 26°E. The CICOS
 208 project, based on the work of various authors (Becker et al., 2014; Bwangoy et al., 2010; Lee
 209 et al., 2011), used an approach proposed by Betbeder et al. (2014) to identify four inundation
 210 zones (Figure 2b) in the central basin; (a) forests inundated for short periods and low
 211 amplitudes at the northern fringes of the Cuvette Centrale and west of the Ubangi river (b) a
 212 permanently inundated swamp forest that encloses the lower Sangha and south of the Likouala
 213 aux Herbes rivers (c) a mosaic of flooded and dry areas north of lake Mai Ndombe (d) another
 214 mosaic of flooded and the dry regions south-east of lake Mai Ndombe. This is in addition to
 215 other seasonally inundated forests at the edges of watercourses.



216

217 **Figure 2.** (a) Outline map of the Congo River basin showing the four main drainage units and
 218 major rivers. Also shown are in situ gauging stations where flow records were obtained, they
 219 are Sangha at Ouessou, Ubangi at Bangui, Lualaba at Kisangani, Kasai at Kutu-Moke and Congo
 220 at Brazzaville/Kinshasa (BZV/KIN). Rivers are Al, Alima; Ar, Aruwimi; Co, Congo; Gr, Giri;
 221 It, Itimbiri; Ks, Kasai; LiM, Likouala Mossaka; LiH, Likouala aux Herbes; Lm, Lomami; Lu,
 222 Lulunga; Ll, Lualaba; Mg, Mongala; Ob, Ubangi; R, Ruki; Sg, Sangha. The black dashed line
 223 encircles the central basin sensu lato while the area shaded with thick diagonal lines is that of
 224 the Batékés Plateaux (adapted from Moukandi N’kaya et al. this volume) and (b) Cuvette
 225 Centrale showing the Ubangi, Giri, Congo, and Ruki Rivers adjacent to seasonally and
 226 permanently inundated areas. Also shown are the locations of Lake Mai Ndombe, within non-
 227 flooded forests, and Lake Tele north of the Likouala aux Herbes River (adapted and generalized
 228 from Betbeder et al. (2014) and BRLi, (2016).

229 The Cuvette Centrale has a complex hydrological system due to the number of tributaries and
 230 swamps that are linked to it. The slopes of the middle reach of the Congo River are as low as
 231 2cm.km^{-1} and run through the Cuvette Centrale (Laraque, 1998a) but steepens to 8 cm.km^{-1} at
 232 the outlet of the Cuvette Centrale (Carr et al., 2019). Several rivers join the main stem at the
 233 middle reach, notably the Mongala, Giri, Ubangi, and Sangha rivers on the northern bank and
 234 the Lulunga, Ikelemba, Kasai, and Ruki rivers on the southern bank. The Ubangi is the second
 235 largest tributary of the Congo River and the main one on the right bank. In contrast, the Kasai
 236 River, which is the main tributary of the Congo River on the left bank, does not feed into the
 237 Cuvette Centrale directly. The lowest point of the Cuvette Centrale occurs at the confluence
 238 where the Congo meets with the Ubangi, Likouala aux Herbes, Sangha, and Likouala Mossaka
 239 (Laraque et al., 1998a). The Cuvette Centrale is bounded to the South by the sandstone aquifers
 240 of the Batekes group of rivers, which serve an important buffering role on the hydrological
 241 cycle well described by Laraque et al. (1998b). Importantly too, the Cuvette Centrale hosts the
 242 single largest peatland complex known in the tropics (Dargie et al., 2017).

243 2.2. Model selection

244 The SWAT model is a physically-based, semi-distributed hydrologic model that has been used
 245 extensively to predict the impact of land management practices on water, sediment, and
 246 agricultural chemical transport (Arnold et al., 1998, 2012). Moreover, SWAT can provide
 247 continuous simulations for dissolved and particulate elements in large and complex catchments
 248 with varying weather, soils, and management conditions over long periods (Arnold et al.,

249 1998). Due to the size and spatial heterogeneities associated with the Congo basin, it was
250 important to choose a model that will consider a majority of the relevant hydrological processes
251 like infiltration, interception, soil moisture, groundwater components as well as attenuation
252 effects of wetlands, ponds, and artificial reservoirs. SWAT has demonstrated its applicability
253 in several regions of the world (Malagó et al., 2017; Zhang et al., 2013) in Africa (Van
254 Griensven et al., 2012) and in the Congo basin (Aloysius et al., 2017). Also, the easy
255 accessibility of basic GIS data that are required as SWAT inputs and the availability of a
256 reliable developer support increases its appeal even in data-scarce areas (Van Griensven et al.,
257 2012; Gasman et al., 2010). This is in stark contrast to models like the *Système Hydrologique*
258 *Européen* (MIKE SHE), which requires extensive model data and physical parameters that may
259 not be available all the time. It also makes the model difficult to set up, coupled with the fact
260 that users are unable to modify the code (Devi et al., 2015). Easton et al. (2010) used the SWAT
261 model to determine runoff and erosion in the Blue Nile basin to find out the respective sources.
262 They found out that only minimal direct calibration is required to obtain good hydrologic
263 predictions. Borah and Bera (2004) have made a comparison between SWAT, Hydrological
264 Simulation Program-Fortran (HSPF) and the Dynamic Watershed Simulation Model (DWSM)
265 models and found 17 applications of SWAT in North America. They concluded that it could
266 be applied for continuous simulations of water flow, sediments, and nutrient transport.
267 Furthermore, SWAT has been successfully used for water quantities (Schuol & Abbaspour,
268 2007), climate change studies (Aloysius and Sainers, 2016), and water quality (Gassman et al.,
269 2007) assessments for a wide range of scales and environmental conditions.

270 2.2.1. Modified parameters for the tropics

271 The SWAT hydrological model was originally developed for temperate regions. The main
272 limitation in its use in tropical areas is related to the simulation of tropical vegetation. SWAT
273 applies dormancy to terminate growing seasons while in the tropics, the wet and dry seasons
274 can only be represented by defining heat unit-specific “plant” and “kill” operations, which are
275 fixed for every year of simulation (Strauch & Volk, 2013). The plant growth component of
276 SWAT is based on the radiation use efficiency approach with empirical parameters. Plant
277 growth can be inhibited by temperature, water, nitrogen, and phosphorus stress. Plant
278 development is based on daily accumulated heat unit values. The heat unit states the stage of
279 plant development. It varies from 0 to 1, 0 indicating the sowing time and 1 the optimal moment
280 for the plant to be harvested. By modifying the plant growth module, an alternative approach
281 was presented in which annual growing cycles were initiated based on changes in soil moisture.
282 A soil moisture threshold was set that automatically triggers new growing seasons for perennial
283 crops during the transition from the wet to the dry seasons. Furthermore, a logistic leaf area
284 decline function was defined that enabled a user to set a minimum leaf area index (LAI).
285 Further details on the procedure can be found in Strauch and Volk (2013).

286 2.2.2. Water Balance

287 The SWAT system is coupled with a geographical information system (GIS) engine that
288 integrates various spatial environmental data, including soil, land cover, climate and
289 topographical features (Arnold et al., 1998). Evapotranspiration can be estimated using either
290 the Penman-Monteith, Priestly-Taylor, or Hargreaves methods. SWAT simulates the
291 hydrology of a catchment in two ways; the land phase and the routing phase. The land phase
292 describes the loading of water, nutrients, and pollutants into the main channel in each subbasin.
293 In contrast, the routing phase is the movement of these substances through the channel
294 watershed network to the outlet of the basin. The simulation of the hydrologic cycle by SWAT
295 is based on the water balance equation:

296
$$SW_t = SW_0 + \sum_{i=1}^t (R_{day} - Q_{surf} - E_a - W_{seep} - Q_{gw})$$

297 where SW_t is the final soil water content (mm water), SW_0 is the initial soil water content in
 298 day i (mm water), t is the time (days), R_{day} is the amount of precipitation in day i (mm water),
 299 Q_{surf} is the amount of surface runoff in day i (mm water), E_a is the amount of evapotranspiration
 300 in day i (mm water), W_{seep} is the amount of water entering the vadose zone from the soil profile
 301 in day i (mm water), and Q_{gw} is the amount of return flow in day i (mm water).

302 In SWAT, each HRU is a closed system with no transfer of water between HRUs. Instead the
 303 processes in the land phase are simulated within individual HRUs and cumulatively summed
 304 to calculate the overall water balance (Neitsch et al., 2012). The water balance in the aquifer
 305 was simulated in SWAT using the linear reservoir method to simulate the groundwater flow.
 306 This method assumes that the groundwater storage and base flow have a linear relationship.
 307 Water in the unsaturated zone is either stored as soil moisture or percolates using a storage
 308 routing technique based on the saturated hydraulic conductivity and field capacity of the soil
 309 profile. A kinematic storage model (Sloan et al., 1984) simulates lateral flow accounting for
 310 variation in conductivity, slope, and water content. As water percolates below this unsaturated
 311 zone, it reaches the shallow aquifer. These processes can be controlled by setting threshold
 312 values in the respective groundwater parameters to regulate the movement of water within
 313 these storages. Further equations relating to other hydrological components can be found in
 314 the SWAT theoretical documentation (Neitch et al., 2011).

315

316 2.2.3. Input Data

317 The primary input data used for the model were freely available data, which included the 90 m
 318 resolution Shuttle Radar Topography Mission (SRTM) topography data from the Consortium
 319 for Spatial Information (CGIAR-CSI). This resolution was chosen considering the size of the
 320 watershed. The land use map was extracted from the Global Land Cover Characterization
 321 (GLCC) database and used to estimate vegetation, anthropogenic influences, and water bodies
 322 in the watershed area. Values of minimum and maximum temperature for the period 1979-2014
 323 were obtained from the Climate Forecast Reanalysis System (CFRS). The Tropical Rainfall
 324 Monitoring Mission (TRMM) precipitation products for the period 1998-2015 were used while
 325 the model simulated all other climate variables. Digital soil data for the study was extracted
 326 from the harmonized digital soil map of the world (HWSD v1.1) produced by the Food and
 327 Agriculture Organization of the United Nations (FAO). This soil database provides data for
 328 16,000 different soil mapping units of two layers containing 30 cm and 30 - 100 cm depth).
 329 The Global Wetland Database (GLWD) provided information on swamps and lakes, while the
 330 source of in situ gauge observations for the five hydrological stations used for model calibration
 331 was from the SO-HYBAM and BRLi report. Table 1 below gives further details of these inputs.

332 The period for the current study (2000 to 2012), is chosen due to the common period of
 333 availability of contemporary meteorological records for all the five stations under
 334 consideration. In addition, (Moukandi N’kaya et al., this volume; Tshitenge Mbuebue et al.,
 335 2015), showed that the trends/breaks or shifts in rainfall could be found in runoff, with a ten-
 336 year time lag in some of the major subbasins. Furthermore, the observed flow records at the
 337 Brazzaville/Kinshasa gauging station is almost equal to the hundred-year interannual modulus
 338 of discharge (Laraque et al., 2001, 2013a; BRLi, 2016).

339

340

341 **Table 1.** SWAT data inputs and observations datasets

Data Type	Period	Resolution	Source
Digital Elevation Model (DEM)		90 m	Consortium for spatial information (https://cgiarcsi.community/data/srtm-90m-digital-elevation-database)
Soil		1 km	Harmonized World Soil Database v 1.1 (http://webarchive.iiasa.ac.at/Research/LUC/External-World-soil-database/HTML/index.html?sb=1)
Land use		1 km	Global Land Cover 2000 database (http://forobs.jrc.ec.europa.eu/products/glc2000/products.php)
TRMM (TMPA) 3B42 V.7 Daily product	1998-2015	0.25°	<u>Multi-satellite precipitation analysis</u> (https://pmm.nasa.gov/data-access/downloads/trmm#) Huffman et al. (2007)
Meteorological data	1979 – 2014	~38 km	Climate Forecast System Reanalysis (CFSR) Model (http://rda.ucar.edu/pub/cfsr.html & http://globalweather.tamu.edu/) Dile and Srinivasan (2014); Fuka et al., (2013)
River discharge	2000 – 2012	Daily	SO-HYBAM (http://www.so-hybam.org/); BRLi (2016)
Supporting data			
Water productivity	2009 – 2018	250m	FAO (https://wapor.apps.fao.org/catalog/WAPOR_2/1)
Global Wetlands database	1992-2000	30x30 second	Lehner and Döll (2004) (https://www.worldwildlife.org/publications)
Geology	2012	0.5°	Global lithological database (Hartmann and Moosdorf, 2012).

342

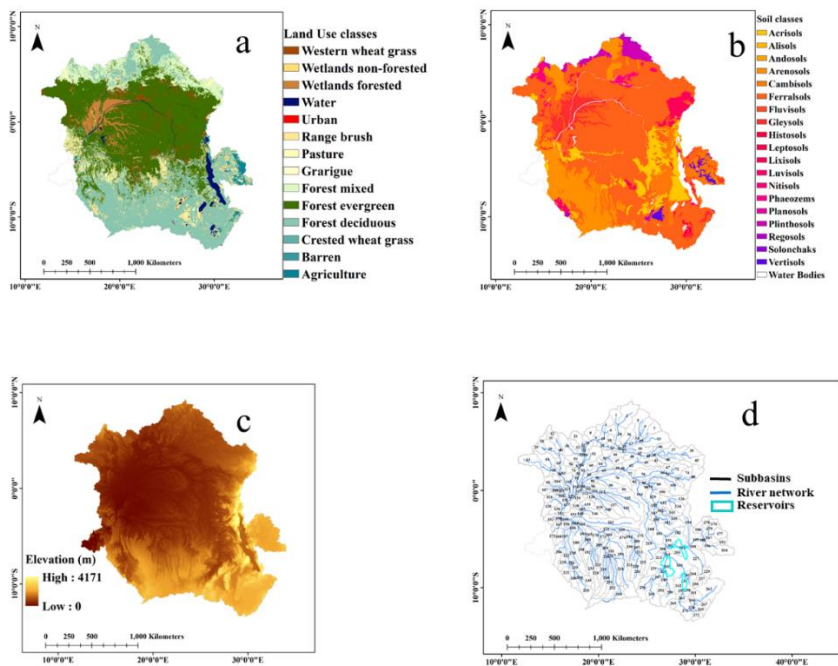
343 **2.2.4. Model setup**

344 The preprocessing of the SWAT model was performed within ESRI ArcGIS 10.4 using the
 345 ArcSWAT interface (www.esri.com). The basin was delineated based on the dominant land
 346 use, soil and slope classes taking into cognizance the size and spatial heterogeneities of the
 347 basin allocating one Hydrologic Response Unit (HRU) per subbasin resulting in 272 subbasins
 348 and HRUs with 20 land use classes and 14 soil classes (Figure 3). The period of simulation was
 349 from 1998 to 2012, comprising calibration (2000-2006), validation (2006-2012), and a two-
 350 year warm-up period (1998-2000) to allow the model to simulate the hydrological cycle
 351 properly. Lakes and wetlands in the upper parts of the Lualaba watershed, which affect the
 352 river discharge substantially, were also integrated into the model. Specifically, they were
 353 placed in subbasins 201, 230, and 238. These subbasins receive flow from Lakes Tanganyika,
 354 Upemba, and Mweru, respectively (see Figure 3d). We also parameterized the reservoirs based
 355 on available information and assuming that no management system was in place (Table 2)

356 **Table 2.** Areas and volumes defined for reservoirs in the SWAT model

Lake name	Subbasin	Surface area (km ²)	Storage Volume (km ³)
Tanganyika	201	32,900	19,000
Upemba	230	550	1.3
Mweru	238	5,000	38

357 The water balance was simulated, and the evapotranspiration calculated using the Penman-
 358 Monteith method. The Penman-Monteith method also gave better estimates of
 359 evapotranspiration when used with the Strauch modified module (section 2.2.1). Minimum and
 360 maximum temperature, wind speed, relative humidity, and solar radiation were other
 361 meteorological data used in combination with the Penman-Monteith. Surface runoff was
 362 simulated using a modification of the soil conservation service Curve Number (CN) method.
 363 The runoff from each subbasin was routed through the river network to the main basin outlet
 364 using the variable storage method. Further theory and details of hydrological processes
 365 integrated into the SWAT model are given by (Arnold et al., 1998; Neitsch et al., 2011) and
 366 are also available online in the SWAT documentation (<http://swatmodel.tamu.edu/>; Neitsch et
 367 al., 2012).



368
 369 **Figure 3.** Main SWAT inputs showing; (a) Land Uses (b) Soil classes (c) Digital Elevation
 370 map and (d) Delineated subbasins of the watershed with locations of Reservoirs as
 371 implemented in ArcSWAT.

2.2.5. Model Calibration

373 The model was calibrated using monthly discharge data from five stations located on major
 374 tributaries of the Congo River. Two of the stations are located on the northern side of the basin
 375 (Ubangi at Bangui and Sangha at Ouesso). In contrast, two are located on the southern side
 376 (Lualaba at Kisangani and Kasai at Kutu-Moke), and the fifth station is located at the
 377 Brazzaville/Kinshasa gauging station that controls 98 percent of the entire catchment. The
 378 stations are evenly distributed and represent (within practical limits) the heterogeneity of the
 379 basin. The common period of calibration for the stations was taken as the years 2000 to 2012
 380 coinciding with the availability of Satellite meteorological data and gauge station observations.

381 The model was calibrated using an iterative (trial and error) method of testing different
 382 parameter values and selecting the best parameter sets. These parameter sets are selected based
 383 on performance criteria that evaluate simulation results against observation data (Werth et al.,
 384 2009). The model was manually calibrated, while parameterization of the model was carefully

385 done by adjusting influential parameters, especially those that are driving forces. Maximum
386 canopy storage (CANMX) was adjusted based on information from the food and agricultural
387 organization (FAO) water productivity (WAPOR) database, while others were adjusted based
388 on local knowledge, e.g. aquifer percolation coefficient (RCHG_DP) and exempted from
389 further calibration (Whittaker et al., 2010; Pagliero et al., 2014). Also, the calibration was
390 regionalized according to the characteristics of the subbasins where in situ data is collected.
391 For instance, revaporation coefficient (GWREVAP) was calibrated based on land use in one
392 region and based on soils in another. The main parameters that were calibrated were the
393 groundwater parameters that have a strong effect on the water retention and transfer between
394 the soil and aquifer as well as the parameters with influence on runoff, infiltration and
395 evapotranspiration.

396 2.2.6. Model Assessment

397 Previous studies in the basin and other global data sets and literature were used to obtain a
398 proper understanding of dominant processes occurring in the basin. Quantitative and qualitative
399 means of assessment were used to evaluate the model performance. For the former, the Nash
400 Sutcliffe efficiency (NSE), the coefficient of determination (R^2), percentage bias (PBIAS) and
401 the Kling-Gupta Efficiency (KGE) were used (Moriassi et al., 2015; Gupta et al., 2009) while
402 the graphical visual assessment was used for a qualitative assessment.

403 2.2.7. Change in Storage

404 A mass balance approach was used to estimate the water balance in the Cuvette Centrale. The
405 change in storage is the difference between the inputs and outputs into and out of the Cuvette
406 Centrale and can be represented as:

$$407 \Delta S = P + Q_i - ET - Q_{out}$$

408 Where S is the change in annual storage, P is the Efficient precipitation over the Cuvette
409 Centrale, Q_i represents the River inflows, ET is Evapotranspiration over the Cuvette Centrale,
410 and Q_{out} represents River outflows in the basin outlet downstream of the Cuvette Centrale after
411 the confluence with the Kasai tributary.

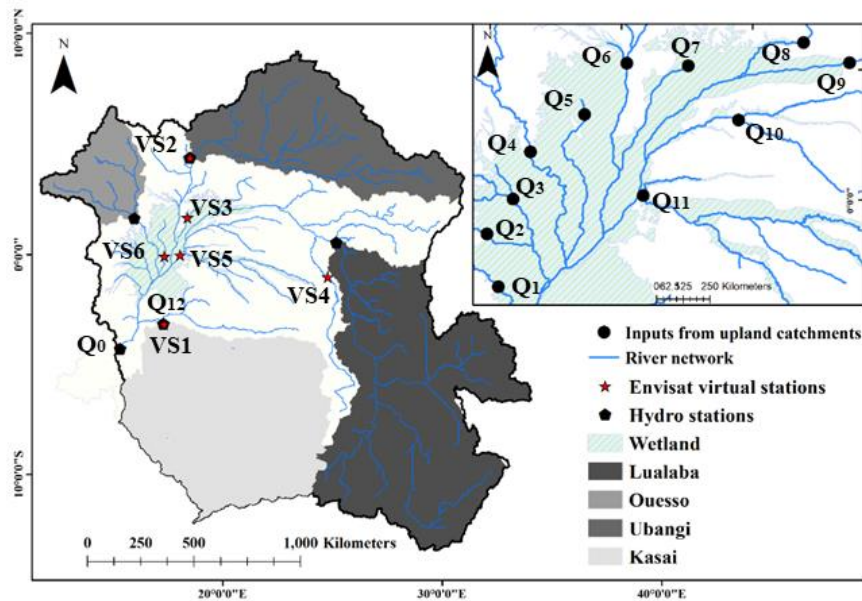
412 Therefore, with respect to Figure 4:

$$413 \Delta S = P + Q_1 + Q_2 + \dots + Q_{11} - ET - (Q_0 + Q_{12})$$

414 Where Q_0 is the discharge at Brazzaville/Kinshasa gauging station in the main stream and Q_{12}
415 discharge from the Kutu-Moke gauging station (Kasai tributary).

416

417 Subbasin outlets were defined during the watershed delineation phase of the project. Outlets
418 were chosen on tributaries that feed into the Cuvette Centrale (see Figure 4).



419

420 **Figure 4.** Close up map of the Cuvette Centrale in the CRB wetlands showing points of inflow
 421 (Q1, Q2...Q11) and outflow (Q0-Q12) used in calculating the wetland water balance. Also
 422 shown are locations of Envisat virtual stations (VS1-VS6) used in validating the model.

423

424 2.3. Envisat Altimetry

425 The Environmental Satellite (ENVISAT) was a mission by the European Space Agency
 426 launched in March 2002 and ended in April 2012. It had a repeat cycle of 35 days and
 427 established virtual stations everywhere its ground tracks intersected a river tributary. From this
 428 database, we were able to validate our model with over 20 virtual stations both within and
 429 outside the Cuvette Centrale, and we present six of such stations in this paper. We used water
 430 surface elevation (WSE) time series from the Theia Hydroweb database (available at
 431 <http://hydroweb.theia-land.fr/>) as a means of validating our model results (Data processing
 432 procedures can be found in Santos da Silva et al. (2010)). The ICE 1 algorithm was used for
 433 processing. Various corrections were applied, including geophysical and environmental
 434 corrections. Height values are corrected for biases specific of each mission/processing
 435 algorithm and then converted into orthometric height by removal of the Earth Gravitational
 436 Model (EGM) 2008 geoidal undulation. The accuracy of altimetry derived water levels over
 437 inland water bodies is estimated to range between 10 and 40–50 cm on rivers (Becker et al.,
 438 2018). The raw ENVISAT data are freely available at the Centre for Topographic studies of
 439 the Oceans and Hydrosphere (CTOH, <http://ctoh.legos.obs-mip.fr/>) in along-track Geophysical
 440 Data Records (GDRs) format. It is worth noting that this dataset was extensively validated in

441 the CRB by Paris et al. (this volume). Surface water elevation from satellite altimetry was
 442 found to provide accurate information on large rivers and even on smaller streams.

443 3. Results and Discussion

444 3.1. Performance of the model

445 Calibration was done at a monthly time step at the outlet of the four main drainage units that
 446 comprise the basin and at the basin outlet. Regional calibration of our model was important to
 447 conserve the peculiar physical characteristics of each drainage basin so as to reflect the
 448 heterogeneity of the entire basin. The model was able to accurately capture the seasonality of
 449 the different subbasins, adequately reflecting the dry and wet seasons as well as years of high
 450 and low discharge. Generally, the model was able to reproduce the timing of floods and
 451 recessions as well as the general shape of the hydrograph, giving a good representation of the
 452 discharge components in each subbasin. The calibration of the Congo basin highlighted the
 453 ability of the SWAT model to separate evaporation and runoff from precipitation at the annual
 454 time scale (see the following section). For this study, we used the performance evaluation
 455 criteria recommended by Moriasi et al. (2007, 2015) in Table 3, which was based on a meta-
 456 analysis of peer-reviewed literature of widely used watershed models, including the SWAT
 457 model to assess our model performance in discharge evaluation. In addition, the KGE statistic
 458 was used (see section 2.2.6). For the calibration period, our ranges of NSE were from 0.16 to
 459 0.81, R^2 from 0.59 to 0.83, PBIAS from -2.11 to 14.52, RSR from 0.43 to 0.99 and KGE from
 460 0.23 to 0.9 while for the validation period NSE was from 0.08 to 0.66, R^2 from 0.39 to 0.78,
 461 PBIAS from -4.10 to 8.19, RSR from 0.58 to 0.75 and KGE from 0.31 to 0.78 (Table 4). Less
 462 acceptable results occurred at the Congo basin outlet and Lualaba subbasins for reasons
 463 discussed in the following sections.

464

465 **Table 3.** Performance evaluation criteria, as suggested by Moriasi et al. (2007, 2015).

Measure	Monthly Performance Evaluation Ranges			
	Very good	Good	Satisfactory	Not satisfactory
R^2	$R^2 > 0.85$	$0.75 < R^2 \leq 0.85$	$0.60 < R^2 \leq 0.75$	$R^2 \leq 0.60$
NSE	$NSE > 0.80$	$0.70 < NSE \leq 0.80$	$0.50 < NSE \leq 0.70$	$NSE \leq 0.50$
PBIAS	$PBIAS < \pm 5$	$\pm 5 \leq PBIAS < \pm 10$	$\pm 10 \leq PBIAS < \pm 15$	$PBIAS \geq \pm 15$
RSR	$0.00 < RSR < 0.50$	$0.50 < RSR < 0.60$	$0.60 < RSR < 0.70$	$RSR > 0.70$

466

467 **Table 4.** Results of the Performance evaluation statistics used in calibration

	Criteria	Ubangi/Bangui	Sangha/Ouessou	Kasai/Kutu-Moke	Lualaba/Kisangani	*BRZ/KIN outlet
Calibration	NSE	0.81	0.67	0.63	0.02	0.16
	R^2	0.83	0.71	0.76	0.49	0.59
	PBIAS	4.01	8.37	-2.11	7.84	14.52
	RSR	0.43	0.57	0.61	0.99	0.92
	KGE	0.90	0.80	0.48	0.23	0.71
Validation	NSE	0.66	0.59	0.59	0.08	0.44
	R^2	0.67	0.65	0.78	0.39	0.54
	PBIAS	-0.86	-1.30	-4.66	-8.19	4.10
	RSR	0.58	0.64	0.64	0.96	0.75
	KGE	0.74	0.78	0.31	0.58	0.73

468 *Brazzaville/Kinshasa

469 Nonetheless, our results compared favorably with other applications in similarly sized
 470 catchments; for instance, Lu et al. (2019) ran the SWAT model in the Yangtze river basin using
 471 CFSR meteorological data and obtained values for streamflow of R^2 and NSE greater than 0.7
 472 in both calibration and validation periods. Gassman et al. (2014) also in an evaluation of 22
 473 large catchments in different continents modeled with SWAT, noted only four studies with R^2
 474 and NSE greater than or equal to 0.9 for both calibration and validation periods on a monthly
 475 time scale. Also, Malago et al. (2017) obtained monthly PBIAS values with a magnitude of not
 476 more than 25 for 70 percent and 60 percent of gauging stations for both calibration and
 477 validation periods, respectively, for their SWAT model in the Danube basin.

478 Aloysius et al. (2017) also ran the SWAT model in the CRB using historical data for the 1950-
 479 2008 period. Their watershed was delineated into 1575 subbasins, which were further divided
 480 into at least 5 HRUs per subbasin. They included sixteen lakes in their model to regulate the
 481 hydrological fluxes applying a power-law relationship. Despite these differences with our
 482 model, they had similar Nash-Sutcliff efficiency values for the Bangui, Brazzaville /Kinshasa,
 483 Kisangani, Kutumoke, and Ouesso, stations of 0.86, 0.34, 0.04, 0.77 and 0.64 respectively for
 484 a similar range of parameters used to calibrate the model (see supplement to Aloysius & Seirs,
 485 2017).

486

487 **Table 5.** Parameters used to calibrate the model for the simulation period

Parameters	Default value	Description	Calibrated range
Groundwater parameters:			
ALPHA_BF	0.048	Base flow alpha factor (days).	0.002-0.016
GWQMN	1,000	Threshold depth of water in the shallow aquifer for return flow to occur (mm).	500-1,000
GW_REVAP	0.12	Groundwater “revap” coefficient	0.02-0.12
REVAPMN	750	Threshold depth of water in the shallow aquifer for “revap” to occur (mm).	0.002
GW_DELAY	31	Groundwater delay time (days).	31
RCHRG_DP	0.05	Deep aquifer recharge	0
HRU parameters:			
CANMX	0	Maximum canopy storage (mm)	50-250
Reach parameters:			
CH_N2	0.014	Manning’s “n” value for the main channel	0.014-0.06
Subbasin parameters:			
CH_N1	0.014	Manning’s “n” value for tributary channels	0.014-0.06

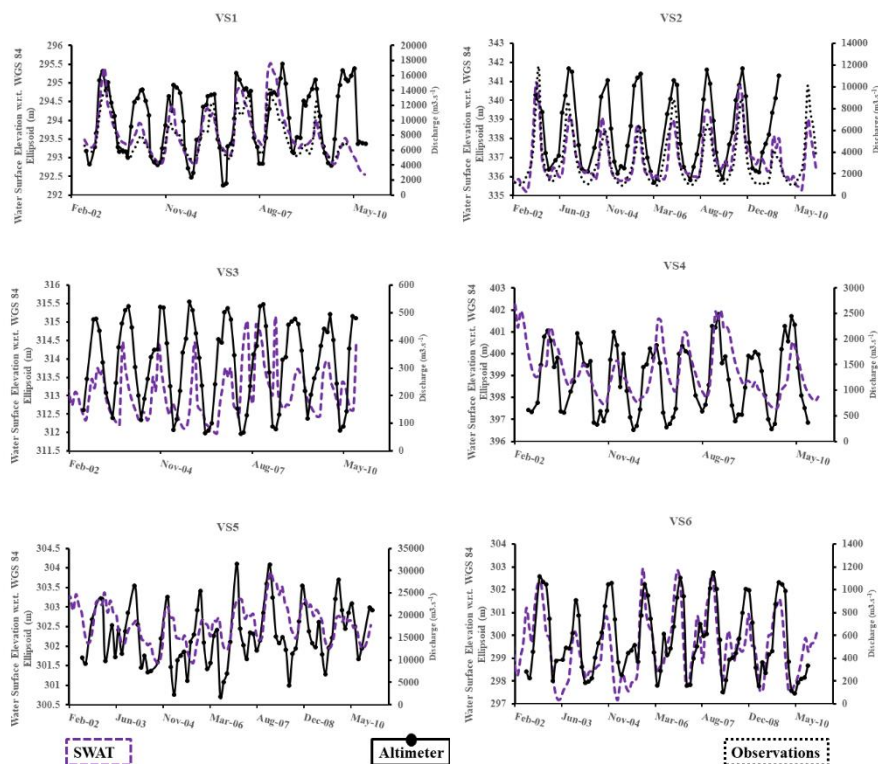
488

489 Table 5 reveals the parameters used to establish the model. They were as much as possible
 490 allowed to retain their physical meaning with the deviation from default values minimized in
 491 order to achieve realistic simulation. Six out of the nine parameter values presented in Table 5,
 492 were groundwater parameters controlling the occurrence, movement, and losses of water from
 493 the system, underlining their importance. This was also noted by Van Griensven et al. (2012)
 494 while reviewing SWAT applications in upper Nile basin countries where they identified 19 out
 495 of 29 parameters that affect hydrological processes and suggested that high values of deep
 496 aquifer recharge parameter (RCHRG_DP) were unrealistic in large basins.

497

498

500 To further validate the applicability of our model in the basin, we made a qualitative
501 comparison between WSE variations from altimetry from 2002 to 2010 and our simulated
502 streamflow. Paris et al. (this volume), extensively validated the WSE dataset used over the
503 Congo basin. Graphs of the satellite altimetry WSE time series compared with modeled
504 discharges for six locations along rivers of different widths (see Table 6) are shown in Figure
505 5. Two of the virtual stations (VS1, VS2) share the same SWAT subbasins where *in situ* gauge
506 stations are located (Kutu-Moke and Bangui, respectively); hence comparisons with observed
507 data were possible. In VS1, two signals from the SWAT model failed to follow the Envisat and
508 observed discharge. This is in contrast to VS2, where the dynamics of the flow components are
509 produced well. This is a reflection of the good calibration at the Bangui station and the less
510 well-reproduced simulation at the Kutu-Moke station and further points to the applicability of
511 altimetry in assessing hydrological model output. Concerning the seasonal observations at the
512 northern and southern drainage units, there is good agreement in peak discharge months, as
513 seen in VS1, VS4 (March/April) and VS2, VS3, and VS6 (October/November) which are
514 representative of both the northern and southern hemispheres respectively. VS5 located on the
515 mainstem Congo River exhibits a second lesser peak characteristic of the flow regimes
516 recorded at the Brazzaville/Kinshasa station. A further look at VS3 is necessary. Indeed, at this
517 VS, the Pearson correlation coefficient was only 0.3, compared to more than 0.6 on the other
518 VSs (Table 6). This decrease in fit between SWE and discharge is noteworthy, and it is due to
519 an error in the precipitation inputs resulting in two peaks of discharge during the low-flow
520 period in 2007 and 2008. These peaks are higher than the peak monthly discharges found in
521 the rest of the study period. Altimetry readings confirm that these two peaks never occurred on
522 this ungauged river during the study period. This particular station highlights the applicability
523 of water stage elevation in validating precipitation products. Satellite-derived precipitation
524 products have been shown to overestimate precipitation due to cloud microphysical processes
525 and moisture distribution in the environment (McCollum et al., 2000). TRMM precipitation
526 products have been known to overestimate high rainfall events and show marked variability in
527 equatorial regions (Beighly et al., 2011; Bharti and Singh, 2015; McCollum et al., 2000;
528 Nicholson et al., 2003). Anomalies could also be caused by errors in sampling arising from
529 sparse gauge network and rainfall amount data or natural variations like El Nino
530 (Huffman, 1997; Iada et al., 2010; Morrissey et al., 1995). A slight temporal shift between stage
531 and discharge is observed in VS4 particularly in 2006; this is a typical behavior of
532 heteroscedasticity in the H-Q relationship due to backwater from the Congo River (see
533 evidence of backwater effect in stage-discharge rating curve from altimetry in Paris et al.
534 (2016)). VS5 is located on the Congo River main stem, upstream the confluences with the
535 Ubangi and the Kasai Rivers. VS5 is located in equatorial regions of the CRB, and it has been
536 shown by Beighly et al. (2011), that Envisat showed inconsistency in variation with streamflow
537 at this region. The comparison with altimetry corroborates what was already discussed, that the
538 upper reach calibration is uncertain due to the lack of data; nevertheless, the good calibration
539 of the Ubangi and Kasai basins leads to a good fit at Brazzaville/Kinshasa. The WSE, as used
540 in this study, confirms that radar altimetry can capture both small and large rivers and can be
541 used where *in situ* data is scarce. Overall, the Envisat stage measurements give some
542 confidence that the simulated discharge is able to represent the hydrology of the Congo River
543 Basin adequately.



545

546 **Figure 5.** Envisat stage measurements compared with simulated and observed discharge (VS1
 547 and VS2) and with simulated discharge (VS3-VS6) at six locations in the Congo basin. Refer
 548 to Figure 4 for locations of the VSs.

549

550 **Table 6.** Characteristics of ENVISAT altimetry stations used in this study. Temporal
 551 coverage period: 2002 to 2010

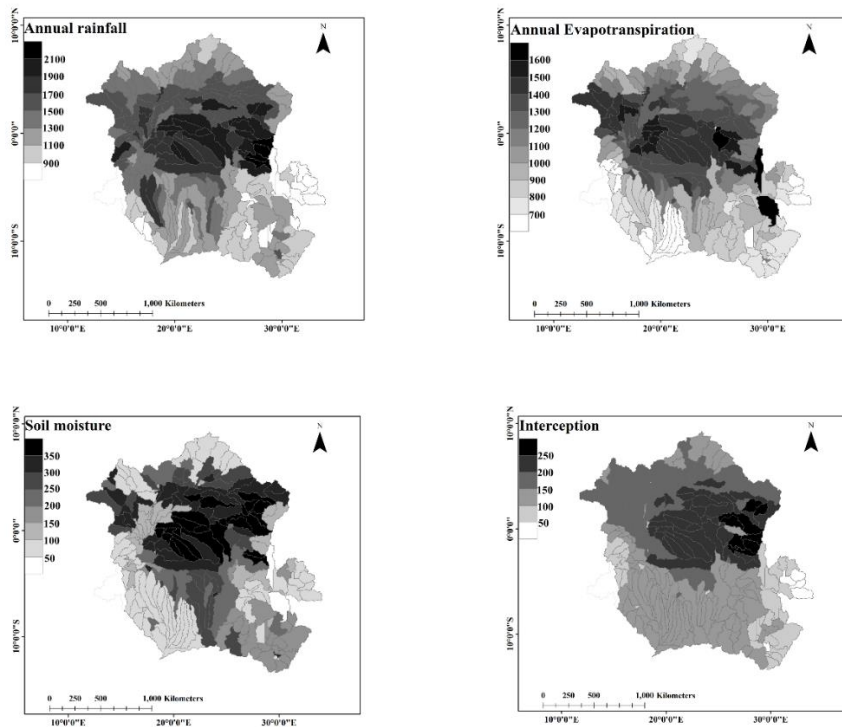
Virtual station Name	Virtual station number	River	Latitude	Longitude	Distance from river mouth (km)	River width (m)	Pearsons correlation coefficient
ENV_930_01	VS1	Kasai	-3.22	17.386	61	1,987	0.61
ENV_343_01	VS2	Ubangi	4.351	18.576	599	1,205	0.76
ENV_887_01	VS3	Giri	1.635	18.454	255	70	0.30
ENV_543_01	VS4	Lomami	-1.083	24.8	398	269	0.66
ENV_429_01	VS5	Congo	-0.072	18.112	1,154	4,461	0.61
ENV_973_01	VS6	Likoula aux Herbes	-0.123	17.404	178	126	0.68

552

553 **3.2. Basin Wide Water Balance**

554 Using the TRMM precipitation data set as input over the entire basin area upstream of the
 555 Brazzaville/Kinshasa gauging station, the model returned an annual average precipitation
 556 amount of 1,510 mm yr⁻¹ with higher rainfall in the central part of the basin (Figure 6a).
 557 Evapotranspiration is returned as 1,058.3 mm yr⁻¹, which translates to about 70 percent of total
 558 annual precipitation. In the same way, the central part of the basin presents higher
 559 evapotranspiration. The lakes zone in the upper parts of the Lualaba River returned high

560 evapotranspiration rates in accordance with the work of Chishugi and Alemaw (2009). Finally,
 561 soil moisture returned various rates along the watershed with an average interannual content of
 562 196 mm yr⁻¹. Potential evapotranspiration was returned as 1,665.5 mm yr⁻¹ for our simulation
 563 period. With regards to infiltration and streamflow, 452.7 mm yr⁻¹ of annual precipitation
 564 percolated to the shallow aquifer, of which 219.49 mm yr⁻¹ returned to make the greatest
 565 contribution to streamflow. Lateral runoff and surface runoff contributed 14.84 mm yr⁻¹ and
 566 131.35 mm yr⁻¹ to streamflow, respectively (Table 7).

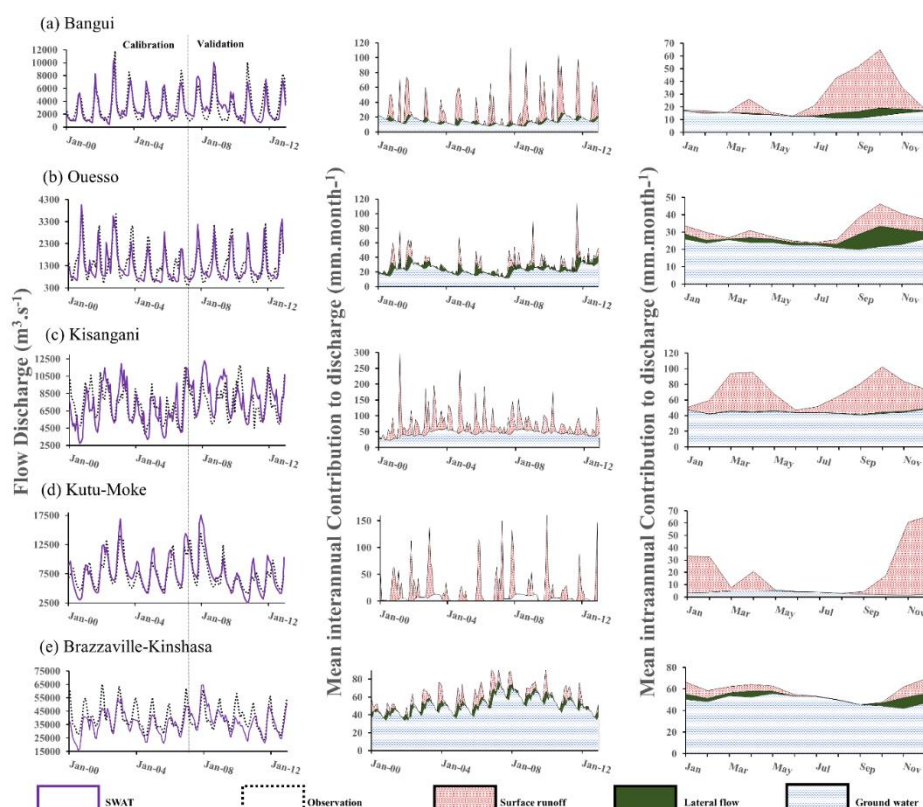


567
 568 **Figure 6.** Maps of mean annual Rainfall, Interception, Evapotranspiration and Soil moisture
 569 for the simulation period 2000-2012. Validated against Chishugi and Alemew (2009).

570
 571 **Table 7.** Annual water balance components for the simulation period 2000-2012 at the outlet
 572 of the basin (Brazzaville/Kinshasa gauging station).

Water balance components	Values (mm yr ⁻¹)	573
Precipitation	1,510.7	574
Actual evapotranspiration	1,058.3	575
Potential evapotranspiration	1,665.5	576
Surface runoff	131.35	577
Lateral flow	14.84	578
Baseflow	219.49	579
Deep aquifer recharge	0	580
		581

583 The Ubangi from its confluence at Mbomou –Uélé to the city of Bangui is 546 km long
 584 (Nguimalet and Orange, 2019) and drains the streams originating from the North of the basin
 585 with the outlet of the drainage unit located about 600 km downstream of the Bangui gauging
 586 station. The monthly averaged interannual discharge simulated at this station was $3,085 \text{ m}^3 \text{ s}^{-1}$
 587 compared to the average observed values of $3,125 \text{ m}^3 \text{ s}^{-1}$ for the 2000 to 2012 period (Table 8).
 588 The overall performance of the model at this outlet was satisfactory to very good for both the
 589 calibration and validation period for most of the performance criteria. The values for the NSE,
 590 R^2 , PBIAS, RSR and KGE are 0.81, 0.83, 4.01, 0.43, 0.90 and 0.66, 0.67, -0.86, 0.58, 0.74 for
 591 both the calibration and validation periods respectively. The reduced efficiency of 0.66 and
 592 negative bias for the validation period results from the overprediction of low and high flows in
 593 the drier years of 2009 and 2010 (Figure 7a). The relatively low contribution of lateral flow to
 594 streamflow corroborates the ferruginous nature of soil characteristics described in the Ubangi
 595 basin (Runge & Nguimalet, 2005). The simulation gave a very good representation of the
 596 magnitude of high and low flows, mimicking the unimodal rainfall pattern observed from
 597 gauge records and reflecting the responsiveness of the Ubangi's flow to the rainfall dynamics
 598 of its catchment area (Nguimalet et al., 2019). It also indicates that most of the processes
 599 occurring in the watershed were being simulated. The simulation at the Ubangi was aided by
 600 the fact that hydrological observations for the northern subbasins of the CRB are relatively
 601 long and of good quality, thus guaranteeing the reliability of results (BRLi, 2016). Generally,
 602 the shape of the hydrograph and the statistical model performance indicate a satisfactory to
 603 very good performance of the SWAT model for the simulation period.



604

605 **Figure 7.** Hydrograph showing the observed and simulated discharge for the calibration (2000-
 606 2012) and validation (2007-2012) period indicated by the broken line. Also shown are the
 607 different contributions of surface, lateral and groundwater flow for the same period. a-e
 608 correspond to the Bangui, Ouesso, Kisangani, Kutu-Moke and Brazzaville/Kinshasa gauging
 609 sites respectively.

610 **Table 8.** Comparison of historical flow with current simulation

Drainage basin	Station	Drainage area km ²	Interannual flow m ³ .s ⁻¹	Specific discharge L s ⁻¹ km ⁻²	Interannual flow (sim)* m ³ s ⁻¹	Interannual flow (obs)* m ³ s ⁻¹	Specific discharge* L s ⁻¹ km ⁻²
Lualaba	Kisangani	974,138	7,640 ¹	7.8	7,323	7,264	7.5
Kasai	Kutu-Moke	750,032	8,070 ²	10.7	7,621	7,365	10.1
Sangha	Ouessou	159,480	1,550 ³	9.7	1,282	1,386	8.03
Ubangi	Bangui	494,088	3,660 ⁴	7.4	3,085	2,931	6.2
Congo	*Bzv/Kin	3,659,897	40,500 ⁵	11.1	36,361	39,963	9.9

611 Periods: ¹: 1951 to 2012; ²: 1940 to 2012; ³: 1948 to 2017 ; ⁴: 1936 to 2017; ⁵: 1903 to 2017. (Data adapted from Moukandi
612 N’kaya et al. (this volume)

613 *current simulation period (2000-2012); obs=observed flow; sim=simulated flow, Bzv/Kin=Brazzaville /Kinshasa

614

615 Like the Ubangi, the modeled discharge at the Sangha station was able to follow the observed
616 hydrograph. It also gave good to satisfactory results for both the calibration and validation
617 periods. Some peaks were overestimated by the model, notably in October 2007 and June 2007.
618 Nonetheless, the model was able to show the steadiness of groundwater flow and the relatively
619 abundant contribution of lateral flow compared to other subbasins (Figure 7b). However, it was
620 not able to adequately represent a series of minor floods that characterizes the flow series in
621 July and August. Of the five sites calibrated, the Sangha basin has the lowest discharge
622 simulated of 1,282 m³ s⁻¹ against an observed discharge of 1,415 m³ s⁻¹ for the period under
623 consideration. It is evident that there are losses here that the model cannot account for. This is
624 illustrated by the huge deficit in simulated flow. Similarly, Munzimi et al. (2019) reported a
625 residual (under-estimate) bias at this station for their subbasin model. They obtained a
626 simulated mean flow of 859 m³.s⁻¹ compared to an observed mean flow of 1,258 m³.s⁻¹ for a
627 similar period to our study. The proximity to floodplains, the inability to capture the minor
628 floods, and the non-integration of wetland processes in both models may account for the
629 reduced response dynamics in this station. This result further illustrates the need for more
630 reliable and improved wetland models in order to reduce biases associated with discharge
631 estimates.

632 The Lualaba drainage subbasin was very complicated to model owing to the presence of many
633 lakes and swamps, including the Tanganyika lake. The Kisangani gauging station is located
634 downstream of these water bodies, and thus it was necessary to integrate reservoirs in our model
635 that will account for attenuation of excess flows. Sub-standard performances were recorded in
636 the Lualaba subbasin for the NSE statistic, which is sensitive to high peaks (Legates et al.,
637 1999). In the Lualaba subbasin, peaks were overestimated in all the years of the validation
638 period (2007-2012) while there was an over and underestimation of peaks in the calibration
639 period (2000-2006) (Figure 7c). We hypothesize that this may be due to the TRMM
640 precipitation products used. For instance, Beighly et al. (2011) showed that TRMM
641 overestimates rainfall in specific periods while Nicholson et al. (2003) highlighted
642 discrepancies in the product compared to gauge observations. The sharp precipitation gradients
643 in the southeastern and adjoining eastern parts of the basin (Tshimanga, 2012) may also be a
644 contributory factor. Nicholson et al. (2019) validated precipitation datasets over the Congo
645 basin western and eastern peripheries. They noted that station density in recent years (1998 to
646 2010) compared to earlier years (1983 to 1994) was much lower and hence contribute to lower
647 performance of precipitation products. However, the modeled discharge of 7,323 m³ s⁻¹
648 compared favorably with the observed discharge of 7,264 m³ s⁻¹ for the simulation period with
649 a difference of less than 1 percent. The discrepancies between the objective functions and the
650 good agreement between the modeled and observed discharge can be explained by the PBIAS.
651 It measures the average tendency of the simulated data to be larger or smaller than the measured

652 ones (Gupta et al., 1999). This will explain the close simulation of the magnitude of the
653 discharge. Nonetheless, the modeling here should be taken with caution and weighed based on
654 the objectives to be achieved.

655 The Kasai subbasin drains the southeastern portions of the Congo basin. Figure 7d shows the
656 simulation results obtained at the Kutu-Moke gauging station that drains the Kasai, the
657 Kwango, and the Kwilo rivers. The model simulated the streamflow components of the Kasai
658 overestimating some peak years (2004, 2006, 2007, 2008, 2011, 2012) and underestimating
659 recessive periods (2000, 2010, 2012), thereby suggesting that more calibration with appropriate
660 model parameters may be possible. The performance evaluation criteria ranged from
661 satisfactory to very good with the regular flows of the Kasai hydrology well simulated. Like
662 the Lualaba basin, we were able to simulate an interannual monthly discharge within 3 percent
663 of the observed value of $7,365 \text{ m}^3 \text{ s}^{-1}$.

664 The Brazzaville/Kinshasa gauging station of the CRB receives flow from most of the tributaries
665 that flow into the Cuvette Centrale as well as the Kasai, Plateaux Batekés Rivers and other
666 tributaries downstream of the Cuvette Centrale. The underprediction of low and peak flows
667 influenced the NSE, which is sensitive to extreme flows. Nevertheless, we captured well the
668 timing of flood events, the bimodal pattern of rainfall over the basin, wet and dry years, and
669 the regularity of groundwater flow over the simulation period (Figure 7e). The relatively high
670 difference between our modeled discharge of $36,360 \text{ m}^3 \text{ s}^{-1}$ to $39,960 \text{ m}^3 \text{ s}^{-1}$ of observed
671 discharge, showing a difference of 9 percent, could be attributed to the attenuation effects of
672 the Cuvette Centrale wetlands. We would need more information about the physical basin
673 characteristics that slow the flow of water in the Cuvette Centrale as well as more information
674 on the hydrological dynamics here in order to improve the simulation. Since we have reliable
675 observed discharge flow records at this site, our results will not be affected.

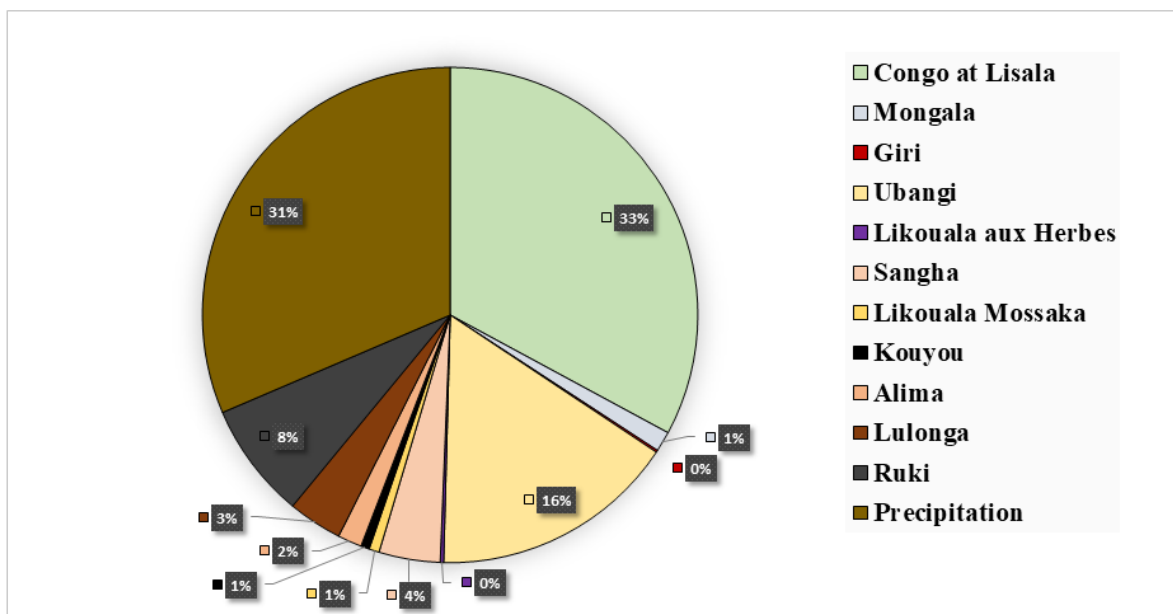
676 3.4. Cuvette Centrale Water Balance

677 To account for all waters that contribute to the central basin, we estimated the total inputs by
678 integrating the precipitation that falls directly on the Cuvette Centrale. This was done by
679 integrating the SWAT subbasins which fall under our wetland area as defined by the Global
680 Wetland Database shape with the streamflow inputs from drainage catchments upstream and
681 around the Cuvette Centrale (Table 9). Points that coincide with historical gauge stations, as
682 documented by Laraque et al. (1995), were used where possible. For the 2000 to 2012 period
683 of our study, we estimated a monthly mean of $34,160 \text{ m}^3 \text{ s}^{-1}$ of water entering the Cuvette
684 Centrale. Considering only flow, we simulated a monthly mean inflow of $24,250 \text{ m}^3 \text{ s}^{-1}$ coming
685 in from the eight tributaries of the right bank (Mongala, Giri, Ubangi, Likouala aux Herbes,
686 Sangha, Likouala Mossaka, Kouyou, Alima), the Congo river at Lisala and two tributaries of
687 the left bank (Lulonga and Ruki). These tributaries have a combined contributing area of
688 $2,191,066 \text{ km}^2$. We were able to capture the seasonality of the flows with a first flood peaking
689 in November and a second lesser one in April. The Congo at Lisala contributes 33 percent of
690 the total inputs, with precipitation almost equaling it at 31 percent. The largest tributary on the
691 right bank – the Ubangi, contributes 16 percent of the total while the left bank tributaries
692 provide 11 percent (Figure 8).

693 **Table 9.** Average monthly interannual simulated inflows and outflows in the Cuvette Centrale from contributing tributaries expressed as flow (m³
694 s⁻¹) for the 2000-2012 period.

	Inputs													Outputs		
	Alima at Tchikapika (Q1)	Kouyou at Linnegue (Q2)	Likouala Mossaka at Makoua (Q3)	Sangha at Ouesso (Q4)	Likouala aux Herbes at Epena (Q5)	Ubangi at Bangui (Q6)	Giri (Q7)	Mongala (Q8)	Congo (Lisala) (Q9)	Lulonga (Q10)	Ruki (Q11)	PPT	Total Inputs	Congo-Kasai (Q0-12)	ETP	Total outputs
Aug	411	147	173	1,047	58	4,206	35	347	8,602	927	1,983	8,224	26,160	25,035	7,289	32,323
Sep	395	140	171	1,850	177	8,641	132	533	8,549	1,028	2,127	12,871	36,614	30,503	6,974	37,477
Oct	446	160	261	2,970	222	9,464	134	880	11,053	1,270	2,732	14,757	44,351	36,563	5,704	42,267
Nov	491	205	442	2,419	172	7,717	95	867	14,350	1,599	3,680	13,278	45,314	44,068	4,147	48,215
Dec	520	216	445	1,447	121	4,619	70	639	15,522	1,470	4,069	8,599	37,738	48,603	3,822	52,426
Jan	526	210	403	1,119	116	3,401	56	470	15,055	1,430	3,760	6,541	33,087	42,473	3,505	45,978
Feb	570	201	352	1,015	106	3,047	51	415	15,115	1,320	3,505	8,250	33,948	31,805	5,622	37,427
Mar	551	187	276	869	75	2,512	44	363	13,029	1,129	2,918	10,642	32,595	26,556	11,429	37,985
Apr	532	201	347	1,076	136	2,860	82	446	14,001	1,324	3,261	11,549	35,815	26,518	8,751	35,270
May	504	180	273	932	74	2,552	43	398	12,692	1,206	2,849	10,364	32,066	27,809	10,203	38,012
Jun	474	173	223	838	65	2,222	53	352	13,256	1,101	2,502	7,435	28,692	26,673	10,254	36,926
Jul	439	157	191	796	62	2,164	37	339	9,798	968	2,191	6,337	23,477	24,580	9,430	34,010
Mean flow	488	181	296	1,365	115	4,450	69	504	12,585	1,231	2,965	9,904	34,155	32,599	7,261	39,860

695



697

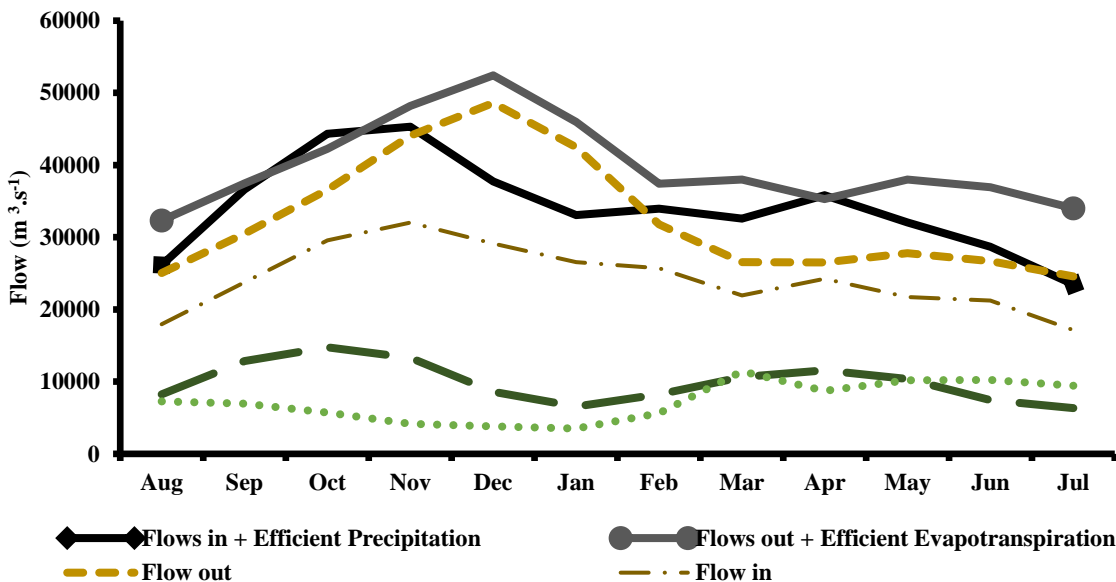
698 **Figure 8.** Pie chart showing the annual mean contribution of Cuvette Centrale tributaries and
 699 efficient precipitation for the period 2000-2012.

700

701 By subtracting the flow recorded at the Kutu-Moke gauging station from the flow recorded at
 702 the Brazzaville/Kinshasa gauging station, we could estimate with a high degree of certainty,
 703 considering the reliability of the gauge records at this site, the flows at the exit of the Cuvette
 704 wetlands. In the same manner, in which we estimated the total inputs, we were able to estimate
 705 the total outputs by also integrating the uptake from evapotranspiration from the subbasins that
 706 comprise the Cuvette Centrale (Table 9). By assuming losses as negligible, we estimated a
 707 monthly mean output from the Cuvette Centrale of $39,860 \text{ m}^3 \text{ s}^{-1}$ or $32,600 \text{ m}^3 \text{ s}^{-1}$ when we take
 708 evapotranspiration into account. A graphical representation of the flows (Figure 9) also shows
 709 we simulated one main flood in December with two relatively lower floods peaking in March
 710 and May.

711 We compared our results with the work of Moukandi et al. (this volume), which is the first
 712 attempt to reconstitute the balance of the Cuvette Centrale. Their work was based on deductions
 713 from a study of the in situ hydrological chronicles of the major drainage features of the Congo
 714 basin. Figure 9 shows similarities with their reconstruction, notably the peak in flows in
 715 December and January and the second flood in May with a dome-shaped peak attributable to
 716 the April-May floods from the Kasai. The small floods of July-August associated with the
 717 Sangha are not decipherable due to the relatively small size of discharge. In any case, their
 718 analysis suggested that from 1971 to 2017, these floods were replaced by a Plateau. Similarly,
 719 the flows in the Ubangi contribute to the floods that begin to rise in September and recede

720 around February, as illustrated in Figure 9. The Ubangi, with the lowest calculated specific
 721 discharge of the tributaries studied, and the most Northern of the studied basins is the most
 722 sensitive to hydroclimatic deterioration and the most fragile in the basin (Laraque et al., 2013b;
 723 Nguimalet, 2017; Nguimalet and Orange, 2013, 2019). These deficiencies from the Ubangi are
 724 augmented by the Flows from the Lualaba and Kasai Rivers and are regulated by the Cuvette
 725 Centrale.



726
 727 **Figure 9.** Average monthly interannual hydrograph of flows in and out, Precipitation falling
 728 and evapotranspiration removed directly from the Cuvette Centrale in the 2000-2012
 729 simulation period.

730

731 An analysis of the variation in the water balance (Table 10) shows that within the simulation
732 period, the balance is in surplus only at the peak of the rainy seasons (October and April).
733 During all other periods (November to March and May to September), the balance is in deficit,
734 implying that at these times, the storage held in groundwater and flooded areas supply the
735 Congo River. Figure 10 shows the trend in water balance over the 2000-2012 period showing
736 a high deficit in the year 2000 and a gradual restoration of balance to equilibrium in 2012. This
737 coincides with the well-documented deficits in precipitation recorded in the Congo basin from
738 the years 1983-2003 (Nguimalet et al., 2019). In addition, an analysis of the Ubangi River at
739 Bangui showed below-average discharge since the year 2000 (Nguimalet et al., 2013). It also
740 suggests that the regulatory role of the Cuvette Centrale during this hydrological cycle has been
741 seriously challenged. Figure 11 shows monthly averages of water balance components in the
742 Cuvette Centrale. Lateral flow is almost nonexistent, while groundwater flow maintains
743 constant levels all year round with no discernible peaks or lows. Surface runoff reflects the
744 bimodal pattern of rainfall in the basin while the total yield increases in October through to
745 December with a peak in November. The total water yield also reflects the bimodal rainfall
746 pattern with increased surges in April. Evapotranspiration and potential evapotranspiration
747 peak in March and July respectively, differing by up to 100 mm in July, signifying longer
748 periods of dryness. The precipitation reflects the seasonal dynamics associated with the basin
749 by a larger flood in October and a lesser one in April. The importance of groundwater in the
750 CRB is particularly highlighted in the Sangha basin and at the Brazzaville/Kinshasa station,
751 where groundwater levels remain consistent throughout the simulation period varying only
752 minimally even during wet and dry years in the Sangha subbasin. Lateral flow is also more
753 pronounced in the Sangha basin compared to any other subbasin. These characteristics of the
754 Sangha basin fit the description of a “fluvial table or shallow aquifer” of low hydraulic
755 gradients (2 cm.km^{-1}) ascribed to the Likouala aux Herbes basin by Laraque et al. (1998b).
756 This is not surprising as the Ouesso station borders the Cuvette Centrale and is proximate to
757 the Likouala aux Herbes basin, where the depth to the groundwater table is likely closer to the
758 surface. In contrast, there is a minimal contribution of lateral flow at the Brazzaville/Kinshasa
759 outlet with groundwater levels varying relatively more, especially in the year 2008. This
760 coincides with high discharge recorded in the Lualaba river at Kisangani and Kasai river at
761 Kutu-Moke in the same year, suggesting an increased contribution from these two southern
762 tributaries. Overall, the groundwater flow of the Congo basin simulated at the basin outlet
763 demonstrated the regulatory effect of the central basin as it receives contributions of various
764 amounts at different seasons of the year, highlighting the obvious linkages between the upland
765 catchments and the wetland system of the Cuvette Centrale. This is very important considering
766 the deficit being experienced by the Northern tributaries of the CRB (Laraque et al., 2013;
767 Nguimalet 2013, 2017, 2019) as well as future landuse and water diversion plans that will have
768 an impact on this system.

769

770

771

772

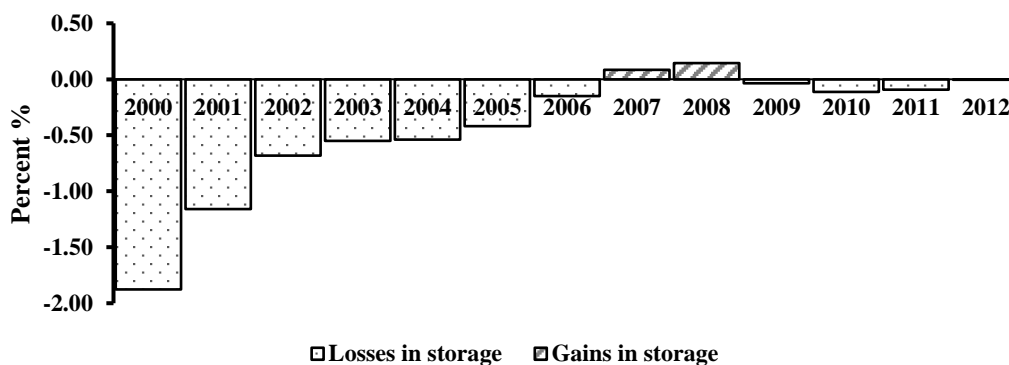
773

774

775 **Table 10.** Average monthly interannual change in storage expressed as flow ($\text{m}^3 \text{s}^{-1}$) for the
 776 2000-2012 period.

	Total inputs	Total outputs	Change in storage
Aug	26,160	32,323	-6,163
Sept	36,614	37,477	-863
Oct	44,351	42,267	2,084
Nov	45,314	48,215	-2,901
Dec	37,738	52,426	-14,688
Jan	33,087	45,978	-12,891
Feb	33,948	37,427	-3,479
Mar	32,595	37,985	-5,390
Apr	35,815	35,270	545
May	32,066	38,012	-5,946
Jun	28,692	36,926	-8,234
Jul	23,477	34,010	-10,533
Mean	34,155	39,860	-5,705

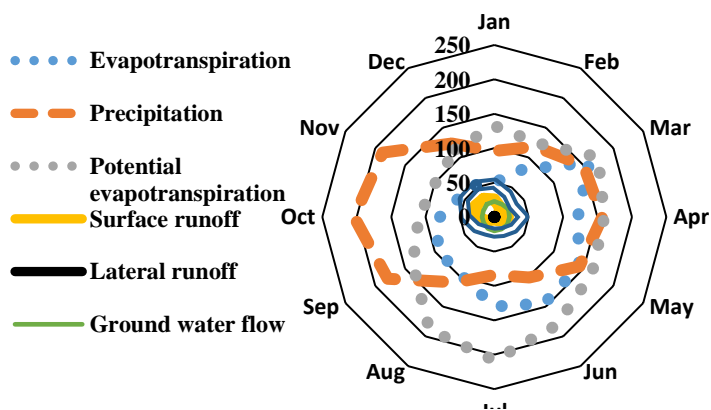
786



787

788 **Figure 10.** Relative interannual change in storage within the Cuvette Centrale for the 2000-
 789 2012 period.

790



791

792 **Figure 11.** Monthly averages of water balance components (in millimeters) within the Cuvette
 793 Centrale for the 2000-2012 simulation period.

794

795 To conclude this section, it is noteworthy to acknowledge that there is an unavoidable
796 uncertainty in input data. Rainfall data tests in Africa and elsewhere have revealed this (Strauch
797 et al., 2012; Tshimanga et al., 2012). Rainfall input uncertainty will, therefore, result in
798 uncertainty in runoff and evapotranspiration as well. The FAO soil data used in this study was
799 primarily prepared for agricultural use, with soil depths not exceeding 100 m. Areas with
800 deeper soils will, therefore, have lower storage capacity resulting in over simulation of peak
801 flows (Tshimanga et al., 2014). The simulations in the subbasins impacted by large lakes and
802 wetlands expose the uncertainties in model structural responses as a result of the over-
803 simplification of assumptions. There are also the unknown parameters of the central basin and
804 the unknown effects of other variables that the model cannot account for. The work of Sun et
805 al.(2016) on surface and ground-water mixing with the SWAT model on the floodplains of the
806 Garonne River is encouraging and can be modified for larger catchments. Therefore, we have
807 no doubt, that by integrating flood plains in our model, we will have much more improved
808 simulations as reflected in those tributaries not impacted by the Cuvette Centrale.

809

810 **4. Conclusion**

811 Using a combination of in situ derived discharge data, satellite precipitation data, and freely
812 available geodatasets, the Congo River basin has been modeled to reflect the spatial and
813 temporal variations in streamflow and its associated components. We have shown that not only
814 does the Cuvette Centrale perform a regulatory role on a seasonal scale between high and low
815 water periods, but also between yearly hydrological cycles. The regional approach to
816 calibration took into account the influence of the Cuvette Centrale and its attenuation effects
817 on downstream flows. This is the first study using the SWAT model that attempts to account
818 for the inflows and outflows of water in the Cuvette Centrale. The importance of groundwater
819 in the basin is further highlighted with a majority of the important parameters used to calibrate
820 the model being groundwater parameters. Groundwater levels in the Cuvette Centrale remain
821 constant and steady all year round and supply the river in times of water deficit. The regulatory
822 effect of the Cuvette Centrale is emphasized by the fact that contributions of different amounts
823 and times from different tributaries feed the Cuvette Centrale. Yet, it is able to balance these
824 inputs and even achieve states of equilibrium at certain peak periods.

825 Furthermore, the hydrological simulation conducted with the SWAT model in our study,
826 emphasized the need to explicitly account for wetland processes in the model. The complex
827 interactions between hydrological processes in the basin with respect to the vegetation, soils,
828 climate, and basin physiography add to the challenges of modeling the CRB. An ideal model
829 should be capable of routing flows through wetland depressions in addition to routing overland,
830 channel, and subsurface flow (McKillop et al., 1999). Additionally, a model should be able to
831 realistically simulate the river-wetland exchange dynamics (Hughes et al., 2014). Future
832 improvements of the model will need to consider a very high-resolution digital elevation model
833 that can capture wetland depressions accurately, and thus estimate with high confidence the
834 flow hydrograph at the outlet of the basin. The spatial variability of the parameters within the
835 various subbasins in our model indicates the extent to which the model represents the
836 hydrological processes. Further testing of the spatial and temporal variability of the basin with
837 appropriate basin parameters and inputs of different resolutions, will be an interesting study
838 (Reggiani et al., 1998). This will also aid in identifying the main factors that limit model
839 performance-whether inappropriate model structure or inaccurate parameter values (Melsen et
840 al., 2016). In addition, future efforts will be made to develop wetland modules that are

841 compatible with the main model, (e.g. Hughes et al., 2014) and can be used in the assessment
842 of a wide variety of ecological functions (Fabre et al., 2020; Guilhen et al., 2020).

843 Throughout the discussion, we have referred to the inherent uncertainties associated with our
844 model. There remains insufficient information to estimate the parameters in the Cuvette
845 Centrale. Validation of model results on the field will go a long way in constraining the wetland
846 parameters and supplying information on basin physiographic conditions, which can improve
847 the model. There is also a need to establish more gauge networks for improved observations.
848 Concerted efforts should also be made to harmonize regional datasets in order to reduce input
849 uncertainties. Furthermore, local researchers should be encouraged through increased funding
850 to make their research more visible and accessible to the global community.

851 The central Congo basin hosts internationally important sites, including the lake Tumba and
852 Mai-Ndombe lakes, parks, and game reserves. While the Cuvette is strongly dependent on
853 upstream year-round surface and groundwater contributions, changes to the wetland hydrology
854 can have negative impacts on the ecology of the wetland as a habitat for fauna and flora. With
855 the ever-increasing demands on natural resources and the collision of various interests within
856 the catchment, there is the need for a harmonization of these interests through sustainable
857 management of Congo basin wetland resources. The objective functions and flow dynamics
858 recreated in tributaries not impacted by the Cuvette Centrale confirm that the SWAT model
859 applied in this study is capable of being used; after taking into account the uncertainties, for
860 the assessment of water resources as well as in experimental studies associated with the hydro-
861 ecological functioning of the basin. The results from this study with the SWAT model
862 demonstrated an appropriate level of performance in estimating the seasonal pattern of water
863 volume fluctuations in the Cuvette Centrale. Given the relative stability of Congo River
864 hydrology as well as the relatively pristine state of the Congo wetlands, models like this one
865 can be used as a baseline for assessing future changes in wetland hydrology. Estimates from
866 streamflow components can also be used to examine eco hydrological relationships in wetlands
867 and the effect of land use on natural wetland features as well as to gauge the sensitivity of
868 wetland communities to hydrological changes.

869

870

871

872

873

874

875

876 **ACKNOWLEDGMENTS**

877 This study has benefitted from hydrological data provided by the SO/HYBAM Observatory
878 and its collaborators (ECHOBACO, SCVEN-GIE, CICOS, UMNG). We also acknowledge the
879 Theia Hydroweb for providing the satellite radar Altimetry database and finally to the AE-
880 FUNAI/Campus France scholarship scheme for funding the Ph.D. studies of the first author in
881 the Laboratoire Écologie Fonctionnelle et Environnement of Toulouse.

882 **5. REFERENCES**

- 883 Alsdorf, D., Beighley, E., Laraque, A., Lee, H., Tshimanga, R., O’Loughlin, F., Mahé, G.,
884 Dinga, B., Moukandi, G., & Spencer, R. G. M. (2016). Opportunities for hydrologic
885 research in the Congo Basin. *Reviews of Geophysics*, 54(2), 378–409.
886 <https://doi.org/10.1002/2016RG000517>
- 887 Aloysius, N., & Saiers, J. (2017). Simulated hydrologic response to projected changes in
888 precipitation and temperature in the Congo River basin. *Hydrology and Earth System
889 Sciences*, 21(8), 4115–4130. <https://doi.org/10.5194/hess-21-4115-2017>
- 890 Aloysius, N. R., Sheffield, J., Saiers, J. E., Li, H., & Wood, E. F. (2016), Evaluation of historical
891 and future simulations of precipitation and temperature in central Africa from CMIP5
892 climate models, *J. Geophys. Res. Atmos.*, 121, 130–152, doi:10.1002/2015JD023656
- 893 Arnold, J.G., Srinivasan, R., Muttiah, R.S., & Williams, J.R. (1998). Large area hydrologic
894 modeling and assessment part 1: model development. *J. Am. Water Resour. Assoc.* 34,
895 73-89. <https://doi.org/10.1111/j.1752-1688.1998.tb05961>
- 896 Arnold, J. G., Kiniry, J. R., Srinivasan, R., Williams, J. R., Haney, E. B., & Neitsch, S. L.
897 (2012). Soil and Water Assessment Tool “SWAT”: Input/Output Documentation. Texas
898 Water Resources Institute, 1068–1068. https://doi.org/10.1007/978-0-387-35973-1_1231
- 899 Becker, M., da Silva, J. S., Calmant, S., Robinet, V., Linguet, L., & Seyler, F. (2014). Water
900 level fluctuations in the Congo Basin derived from ENVISAT satellite altimetry. *Remote
901 Sensing*, 6(10), 9340–9358. <https://doi.org/10.3390/rs6109340>
- 902 Becker, M., Papa, F., Frappart, F., Alsdorf, D., Calmant, S., da Silva, J. S., Prigent, C., & Seyler,
903 F. (2018). Satellite-based estimates of surface water dynamics in the Congo River Basin.
904 *International Journal of Applied Earth Observation and Geoinformation*, 66(August

2017), 196–209. <https://doi.org/10.1016/j.jag.2017.11.015>

Beighley, R. E., Ray, R. L., He, Y., Lee, H., Schaller, L., Andreadis, K. M., Durand, M., Alsdorf, D. E., & Shum, C. K. (2011). Comparing satellite derived precipitation datasets using the Hillslope River Routing (HRR) model in the Congo River Basin. *Hydrological Processes*, 25(20), 3216–3229. <https://doi.org/10.1002/hyp.8045>

Betbeder, J., Gond, V., Frappart, F., Baghdadi, N. N., Briant, G., & Bartholome, E. (2014). Mapping of central africa forested wetlands using remote sensing. *IEEE Journal of Selected Topics in Applied Earth Observations and Remote Sensing*, 7(2), 531–542. <https://doi.org/10.1109/JSTARS.2013.2269733>

Bernard, E. (1945). Climat écologique de la Cuvette Centrale Congolaise Institut national pour l'étude agronomique du Congo. In: Sandenson, M. (1949). *Ecology*, 30(2), 265–269. <https://doi:10.2307/1931200>

Bernard-Jannin, L., Brito, D., Sun, X., Jauch, E., Neves, R., Sauvage, S., & Sánchez-Pérez, J. M. (2016). Spatially distributed modelling of surface water-groundwater exchanges during overbank flood events - a case study at the Garonne River. *Advances in Water Resources*, 94, 146–159. <https://doi.org/10.1016/j.advwatres.2016.05.008>

Bharti, V., & Singh, C. (2015), Evaluation of error in TRMM 3B42V7 precipitation estimates over the Himalayan region, *Journal of Geophysical Research Atmosphere*, 120(12), 458–12,473, <https://doi:10.1002/2015JD023779>

Borah, D.K. & Bera, M. (2004). Watershed-scale hydrologic and nonpoint-source pollution models: review of application. *American Society of Agricultural Engineers* ISSN 0001–2351. Vol. 47(3): 789–803.

Borges, A. V., Abril, G., Darchambeau, F., Teodoru, C. R., Deborde, J., Vidal, L. O.,

928 Lambert, T., & Bouillon, S. (2015). Divergent biophysical controls of aquatic CO₂ and
929 CH₄ in the World's two largest rivers. *Scientific Reports*, 5, 1–10.
930 <https://doi.org/10.1038/srep15614>

931 Bouillon, S., Yambélé, A., Gillikin, D. P., Teodoru, C., Darchambeau, F., Lambert, T., &
932 Borges, A. V. (2014). Contrasting biogeochemical characteristics of right-bank
933 tributaries and a comparison with the mainstem Oubangui River, Central African
934 Republic (Congo River basin). *Scientific Reports*, 4(5402), 10–1038.

935 BRLi. (2016) : Développement et mise en place de l'outil de modélisation et d'allocation des
936 ressources en eau du Bassin du Congo : Rapport technique de construction et de calage du
937 modèle, CICOS, Kinshasa, RDC. <https://www.cicos.int>

938 Bultot, F. (1971). Atlas Climatique du Bassin Congolais Publications de L'Institut National
939 pour L'Etude Agronomique du Congo (I.N.E.A.C.), Deuxieme Partie, Les Composantes
940 du Bilan d'Eau.

941 Bwangoy, J. R. B., Hansen, M. C., Potapov, P., Turubanova, S., & Lumbuenamo, R. S. (2013).
942 Identifying nascent wetland forest conversion in the Democratic Republic of the Congo.
943 *Wetlands Ecology and Management*, 21(1), 29–43. [https://doi.org/10.1007/s11273-012-](https://doi.org/10.1007/s11273-012-9277-z)
944 [9277-z](https://doi.org/10.1007/s11273-012-9277-z)

945 Bwangoy, J. R. B., Hansen, M. C., Roy, D. P., Grandi, G. De, & Justice, C. O. (2010). Wetland
946 mapping in the Congo Basin using optical and radar remotely sensed data and derived
947 topographical indices. *Remote Sensing of Environment*, 114(1), 73–86.
948 <https://doi.org/10.1016/j.rse.2009.08.004>

949 Carr, A. B., Trigg, M. A., Tshimanga, R. M., Borman, D. J., & Smith, M. W. (2019). Greater
950 water surface variability revealed by new Congo River field data: Implications for satellite

951 altimetry measurements of large rivers. *Geophysical Research Letters*, 46(14), 8093–
952 8101. <https://doi.org/10.1029/2019GL083720>

953 Chishugi, J.B. & Alemaw, B.F. (2009). The hydrology of the Congo River Basin: A GIS-based
954 hydrological water balance model. In: S. Starrett, ed. *World environmental and water
955 resources congress 2009: great rivers*. Reston, Virginia: American Society of Civil
956 Engineers, 1–16.

957 Dargie, G. C., Lewis, S. L., Lawson, I. T., Mitchard, E. T. A., Page, S. E., Bocko, Y. E., & Ifo,
958 S. A. (2017). Age, extent and carbon storage of the central Congo Basin peatland complex.
959 *Nature*, 542(7639). <https://doi.org/10.1038/nature21048>

960 Davidson, N. C. (2014). How much wetland has the world lost? Long-term and recent trends
961 in global wetland area. *Marine and Freshwater Research*, 65(10), 934–941.
962 <https://doi.org/10.1071/MF14173>

963 Davies B.R., & Gasse F. (1987.). *African wetlands and shallow water bodies - Zones humides
964 et lacs peu profonds d’Afrique*, ORSTOM, Paris, 1987, 650 p.

965 Devi, G. K., Ganasri, B. P., & Dwarakish, G. S. (2015). A Review on Hydrological Models.
966 *Aquatic Procedia*, 4, 1001-1007. <https://dx.doi.org/10.1016/j.aqpro.2015.02.126>

967 Dile, Y. T., & Srinivasan, R. (2014). Evaluation of CFSR climate data for hydrologic prediction
968 in data-scarce watersheds: An application in the Blue Nile River Basin. *Journal of the
969 American Water Resources Association*, 50(5), 1226–1241.
970 <https://doi.org/10.1111/jawr.12182>

971 Easton, Z. M., Fuka, D. R., White, E. D., Collick, A. S., Biruk Ashagre, B., McCartney, M.,
972 Awulachew, S. B., Ahmed, A. A., & Steenhuis, T. S. (2010). A multi basin SWAT

973 model analysis of runoff and sedimentation in the Blue Nile, Ethiopia. *Hydrology and*
974 *Earth System sciences*, 14, 1827–1841, doi:10.5194/hess-14-1827-2010, 2010

975 Farr, T.G., Caro, E., Crippen, R., Duren, R., Hensley, S., Kobrick, M., Paller, M., Rodriguez,
976 E., Rosen, P., Roth, L., Seal, D., Shaffer, S., Shimada, J., Umland, J., & Werner M.
977 (2007). The Shuttle Radar Topography Mission. *Reviews of Geophysics*, volume 45,
978 RG2004, doi:10.1029/2005RG000183

979 Fabre, C., Sauvage, S., Guilhen, J., Cakir, R., Gerino, M., & Sánchez-Pérez, J. M. (2020).
980 Daily denitrification rates in floodplains under contrasting pedo-climatic and
981 anthropogenic contexts: Modelling at the watershed scale. *Biogeochemistry*, 4, 317–
982 336. <https://doi.org/10.1007/s10533-020-00677-4>

983 Forsberg, B. R., Araujo-Lima, C. A. R. M., Martinelli, L. A., Victoria, R. L., & Bonassi, J. A.
984 (1993). Autotrophic Carbon Sources for Fish of the Central Amazon. *Ecology*, 74(3),
985 644–652. <https://doi.org/10.2307/1940793>

986 Gassman, P. W., Reyes, M. R., Green, C. H., & Arnold, J. G. (2007). The Soil and Water
987 Assessment Tool: Historical development, applications, and future research directions.
988 *Transactions of the ASABE*, 50(4): 1211-1250. doi: 10.13031/2013.23637)

989 Gassman, P. W., Sadeghi, A. M., & Srinivasan, R. (2014). Applications of the SWAT model
990 special section: Overview and insights. *Journal of Environmental Quality*, 43(1), 1–8.
991 <https://doi.org/10.2134/jeq2013.11.0466>

992 Gassman, P.W., Arnold, J.G., Srinivasan, R., & Reyes, M. (2010). The worldwide use of the
993 SWAT model: Technological drivers, networking impacts, and simulation trends. In
994 *Proceedings of the conference-21st Century Watershed Technology: Improving Water*
995 *Quality and Environment*, Universidad EARTH, Costa Rica, February 21-24

- 996 2010.ASABE Publication No. 701P0210cd. doi:10.13031/2013.29418
- 997 Guilhen, J., Al Bitar, A., Sauvage, S., Parrens, M., Martinez, J.-M., Abril, G., Moreira-Turcq,
998 P., & Sanchez-Pérez, J.-M.(2020) Denitrification, carbon and nitrogen emissions over the
999 Amazonian wetlands, Biogeosciences, <https://doi.org/10.5194/bg-2020-3>
- 1000 Gupta, H. V., Kling, H., Yilmaz, K. K., & Martinez, G. F. (2009). Decomposition of the mean
1001 squared error and NSE performance criteria: Implications for improving hydrological
1002 modelling. *Journal of Hydrology*, 377(1–2), 80–91.
1003 <https://doi.org/10.1016/j.jhydrol.2009.08.003>
- 1004 Haensler, A., Jacob, D., Kabat, P., & Ludwig, F. (2013). Assessment of projected climate
1005 change signals over central Africa based on a multitude of global and regional climate
1006 projections. *Climate Change Scenarios for the Congo Basin*. Retrieved from
1007 www.climate-service-center.de/imperia/md/content/csc/csc-report11_optimized.pdf.
- 1008 Hartmann, J., & Moosdorf N.(2012). The new global lithological map database GLiM: A
1009 representation of rock properties at the Earth surface, *Geochemistry, Geophysics,*
1010 *Geosystems*, 13, Q12004, doi:10.1029/2012GC004370
- 1011 Huffman,G.J., Adler R.F., Bolvin, D.T., Gu, G.J., Nelkin, E.J., Bowman, K.P., Hong, Y.,
1012 Stocker, E.F., & Wolff, D.B. (2007). The TRMM multisatellite precipitation analysis
1013 (TMPA): Quasi-global, multiyr, combined-sensor precipitation estimates at fine scales.
1014 *Journal of Hydrometeorology*, 8: 38–55.
- 1015 Hughes, D. A., Tshimanga, R. M., Tirivarombo, S., & Tanner, J. (2014). Simulating wetland
1016 impacts on stream flow in southern Africa using a monthly hydrological model.
1017 *Hydrological Processes*, 28(4), 1775–1786. <https://doi.org/10.1002/hyp.9725>
- 1018 Iida, Y., Kubota, T., Iguchi, T., & Oki, R. (2010). Evaluating sampling error in TRMM/PR

1019 rainfall products by the bootstrap method: Estimation of the sampling error and its
1020 application to a trend analysis, *Journal of Geophysical Research*, 115, D22119,
1021 doi:10.1029/2010JD014257

1022 Jung, H. C., Hamski, J., Durand, M., Alsdorf, D., Hossain, F., Lee, H., Azad
1023 Hossain,A.K.M.,Hasan,k., Saleh Khan,A. & Zeaul Hoque, A. K. M. (2010).
1024 Characterization of complex fluvial systems using remote sensing of spatial and temporal
1025 water level variations in the Amazon, Congo, and Brahmaputra rivers. *Earth Surface
1026 Processes and Landforms*, 35(3), 294–304. <https://doi.org/10.1002/esp.1914>

1027 Keddy, P. A., Fraser, L. H., Solomeshch, A. I., Junk, W. J., Campbell, D. R., Arroyo, M. T. K.,
1028 & Alho, C. J. R. (2009). Wet and Wonderful: The World’s Largest Wetlands Are
1029 Conservation Priorities. *BioScience*, 59(1), 39–51.
1030 <https://doi.org/10.1525/bio.2009.59.1.8>

1031 Kim, D., Lee, H., Laraque, A., Tshimanga, R. M., Yuan, T., Jung, H. C.,Beighly,E., & Chang,
1032 C. H. (2017). Mapping spatio-temporal water level variations over the central congo river
1033 using palsar scansar and envisat altimetry data. *International Journal of Remote Sensing*,
1034 38(23). <https://doi.org/10.1080/01431161.2017.1371867>

1035 Kim, D., Yu, H., Lee, H., Beighley, E., Durand, M., Alsdorf, D. E., & Hwang, E. (2019).
1036 Ensemble learning regression for estimating river discharges using satellite altimetry data:
1037 Central Congo River as a Test-bed. *Remote Sensing of Environment*, 221(December
1038 2018), 741–755. <https://doi.org/10.1016/j.rse.2018.12.010>

1039 Kugler, Z., Nghiem, S. V., & Brakenridge, G. R. (2019). L-band passive microwave data from
1040 SMOS for river gauging observations in tropical climates. *Remote Sensing*, 11(7).
1041 <https://doi.org/10.3390/RS11070835>

- 1042 Laraque, A., Bellanger, M., Adèle, G., Guebanda, S., Gulemvuga, G., Pandi, A., Paturel, J. E.,
1043 Robert, A., Tathy, J. P. & Yambele, A. (2013a). Recent evolution of Congo, Oubangui and
1044 Sangha Rivers flows. *International journal of tropical geology, geography and ecology.*,
1045 37(1), 93–100.
- 1046 Laraque, A., Bricquet, J. P., Pandi, A. & Olivry J. C. (2009), A review of material transport by
1047 the Congo River and its tributaries, *Hydrological Processes*, 23, 3216–3224,
1048 doi:10.1002/hyp.7395
- 1049 Laraque, A., Castellanos, B., Steiger, J., Lòpez, J.L., Pandi, A., Rodriguez, M. , Rosales, J. ,
1050 Adèle, G., Perez, J., & C. Lagane (2013b), A comparison of the suspended and dissolved
1051 matter dynamics of two large inter-tropical rivers draining into the Atlantic Ocean: the
1052 Congo and the Orinoco. *Hydrol. Process.* 27, 2153–2170. doi:10.1002/hyp.9776
- 1053 Laraque, A., Mahé, G., Orange, D. & B. Marieu (2001), Spatiotemporal variations in
1054 hydrological regimes within Central Africa during the XXth century, *Journal of*
1055 *Hydrology*, 245, 104–117.
- 1056 Laraque, A. & Maziezoula B. (1995). Banque de données hydrologiques des affluents
1057 Congolais du fleuve Congo-Zaire et informations physiographiques, —Programme
1058 PEGI/GBF, pp. 250, Volet Congo - UR22/DEC, ORSTOM - Laboratoire d'hydrologie,
1059 Montpellier, 157 p.
- 1060 Laraque, A., Mietton, M., Olivry, J. C., & Pandi A. (1998a). Impact of lithological and vegetal
1061 covers on flow discharge and water quality of Congolese tributaries from the Congo River,
1062 *Journal of Water Science*, 11, 209–224.
- 1063 Laraque, A., Pouyaud, B., Rocchia, R., Robin, R., Chaffaut, I., Moutsambote, J.-M.,
1064 Maziezoula, B., Censier, C., Albouy, Y., Elenga, H., Etcheber, H., Delaune, M., Sondag,

1065 F., & Gasse F., (1998b). Origin and function of a closed depression in equatorial humid
1066 zones: the lake Tele in north Congo. *Journal of Hydrology* 207, 236–253.

1067 Lee, H., Beighley, R. E., Alsdorf, D., Jung, H. C., Shum, C. K., Duan, J., Guo, J., Yamakazi, D.
1068 & Andreadis, K. (2011). Characterization of terrestrial water dynamics in the Congo Basin
1069 using GRACE and satellite radar altimetry. *Remote Sensing of Environment*, 115(12),
1070 3530–3538. <https://doi.org/10.1016/j.rse.2011.08.015>

1071 Legates, D. R., & McCabe, G. J. (1999). Evaluating the use of “goodness-of-fit” measures in
1072 hydrologic and hydroclimatic model validation. *Water Resources Research*, 35(1), 233-
1073 241. <http://dx.doi.org/10.1029/1998WR900018>

1074 Lehner, B., & Döll, P. (2004). Development and validation of a global database of lakes, res-
1075 ervoires and wetlands. *Journal of Hydrology*, 296, 1–22. <http://dx.doi.org/10.1016/j.jhydrol.2004.03.028>

1077 Lu, J. Z., Zhang, L., Cui, X. L., Zhang, P., Chen, X. L., Sauvage, S., & Sanchez-Perez, J. M.
1078 (2019). Assessing the climate forecast system reanalysis weather data driven hydrological
1079 model for the Yangtze river basin in China. *Applied Ecology and Environmental*
1080 *Research*, 17(2), 3615–3632. https://doi.org/10.15666/aeer/1702_36153632

1081 Malagó, A., Bouraoui, F., Vigiak, O., Grizzetti, B., & Pastori, M. (2017). Modelling water and
1082 nutrient fluxes in the Danube River Basin with SWAT. *Science of the Total Environment*,
1083 603–604, 196–218. <https://doi.org/10.1016/j.scitotenv.2017.05.242>

1084 Melsen, L., Teuling, A., Torfs, P., Zappa, M., Mizukami, N., Clark, M., & Uijlenhoet, R.
1085 (2016). Representation of spatial and temporal variability in large-domain hydrological
1086 models: Case study for a mesoscale prealpine basin. *Hydrology and Earth System*
1087 *Sciences Discussions*, (January), 1–38. <https://doi.org/10.5194/hess-2015-532>

- 1088 McCollum, J.R., Gruber, A., & Ba, M.B. (2000). Discrepancy between gauge and satellite
1089 estimates of rainfall in equatorial Africa. *Journal of Applied Meteorology* 39: 666–679.
- 1090 Mckillop, R., Kouwen, N., & Soulis, E. D. (1999). Modeling the rainfall-runoff response of a
1091 headwater wetland. *Water Resources Research*, 35(4), 1165–1177.
- 1092 Moriasi, D.N.; Arnold, J.G.; Van Liew, M.W.; Bingner, R.L.; Harmel, R.D.; & Veith,
1093 T.L.(2007). Model Evaluation Guidelines for Systematic Quantification of Accuracy in
1094 Watershed Simulations. *Transactions of the ASABE* 2007, 50, 885–900,
1095 doi:10.13031/2013.23153
- 1096 Moriasi, D. N., Gitau, M. W., Pai, N., & Daggupati, P. (2015). Hydrologic and Water Quality
1097 Models: Performance Measures and Evaluation Criteria. *Transactions of the ASABE*,
1098 58(6), 1763–1785. <https://doi.org/10.13031/trans.58.10715>
- 1099 Morrissey, M. L., Maliekal, J. A., Greene, J. S., & Wang, J. (1995). The uncertainty in simple
1100 spatial averages using rain gauge networks. *Water Resources Research*, 31, 2011–2017.
- 1101 Moukandi N’kaya, G.D., Laraque, A., Paturol, J.M, Gulemvuga, G., Mahé, G., & Tshimanga
1102 Muamba, R. (under review). A new look at hydrology in the Congo Basin, based on the
1103 study of multi-decadal chronicles. In *Congo Basin Hydrology, Climate, and*
1104 *Biogeochemistry: A Foundation for the Future*, Alsdorf, D., Tshimanga Muamba, R.
1105 Moukandi N’kaya, G.D., eds, AGU, John Wiley & Sons Inc.
- 1106 Munzimi, Y. A., Hansen, M. C., & Asante, K. O. (2019). Estimating daily streamflow in the
1107 Congo Basin using satellite-derived data and a semi-distributed hydrological model.
1108 *Hydrological Sciences Journal*, 64(12), 1472–1487.
1109 <https://doi.org/10.1080/02626667.2019.1647342>
- 1110 Neitsch, S., Arnold, J., Kiniry, J., & Williams, J. (2011). *Soil & Water Assessment Tool*

- 1111 Theoretical Documentation Version 2009. Texas Water Resources Institute, 1–647.
1112 <https://doi.org/10.1016/j.scitotenv.2015.11.063>
- 1113 Nguimalet, C. R. (2017). Changements enregistrés sur les extrêmes hydrologiques de
1114 l'Oubangui à Bangui (République centrafricaine) : Analyse des tendances. *Revue des*
1115 *Sciences de l'Eau*, 30 (3), 183–196.
- 1116 Nguimalet, C. R. & Orange, D. (2013). Dynamique hydrologique récente de l'Oubangui à
1117 Bangui (Centrafrique): Impacts anthropiques ou climatiques ?" *Revue internationale de*
1118 *géologie, de géographie et d'écologie tropicales*, 37, Tome 1, pp. 101-112.
- 1119 Nguimalet, C. R. & Orange, D. (2019). Caractérisation de la baisse hydrologique actuelle de la
1120 rivière Oubangui à Bangui, République Centrafricaine. *La Houille Blanche*, n° 1, 2019, p.
1121 1-7.
- 1122 Nicholson, S. E., Klotter, D., Zhou, L., & Hua, W. (2019). Validation of satellite precipitation
1123 estimates over the Congo Basin. *Journal of Hydrometeorology*, 20(4), 631–656.
1124 <https://doi.org/10.1175/JHM-D-18-0118.1>
- 1125 Nicholson, S. E., Some, B., McCollum, J., Nelkin, E., Klotter, D., Berte, Y., Diallo, B.M.,
1126 Gaye, I., Kpabeba, G., Ndiaye, O., Noukpozounko, J.N., Tanu, M.M., Thiam, A., Toure,
1127 A.A., & Traore, A.K. (2003). Validation of TRMM and other rainfall estimates with a
1128 high-density gauge dataset for West Africa. Part II: Validation of TRMM rainfall
1129 products. *Journal of Applied Meteorology*, 42(10), 1355–1368.
- 1130 O'Loughlin, F., Trigg, M. A., Schumann, G. J. P., & Bates, P. D. (2013). Hydraulic
1131 characterization of the middle reach of the Congo River. *Water Resources Research*,
1132 49(8), 5059–5070. <https://doi.org/10.1002/wrcr.20398>
- 1133 Papa, F., Durand, F., Rossow, W. B., Rahman, A., & Bala, S. K. (2010). Satellite altimeter-

1134 derived monthly discharge of the Ganga-Brahmaputra River and its seasonal to
1135 interannual variations from 1993 to 2008. *Journal of Geophysical Research: Oceans*,
1136 115(12), 1–19. <https://doi.org/10.1029/2009JC006075>

1137 Pagliero, L.; Bouraoui, F.; Willems, P.; & Diels, J. (2014). Large-Scale Hydrological
1138 Simulations Using the Soil Water Assessment Tool, Protocol Development, and
1139 Application in the Danube Basin. *Journal of Environmental Quality*. 2014, 4, 145–154.

1140 Paris, A., Dias de Paiva, R., Santos daSilva, J., Medeiros Moreira, D., Calmant, S., Garambois,
1141 P.A., Collischonn, W., Bonnet, M.-P., & Seyler F. (2016). Stage-discharge rating curves
1142 based on satellite altimetry and modeled discharge in the Amazon basin, *Water Resources*
1143 *Research*, 52, 3787–3814, doi:10.1002/2014WR016618

1144 Paris, A., Calmant, S., Gosset, M., Fleischmann, A., Conchy, T., Garambois, P.-A., Bricquet,
1145 J.-P., Papa, F., Tshimanga, R., Gulemvuga, G., Laraque, A., Siqueira, V., Tondo, B.,
1146 Paiva, R., & Santos da Silva, J. [under review]. Monitoring hydrological variables from
1147 remote sensing and modelling in the Congo River basin. In *Congo Basin Hydrology,*
1148 *Climate, and Biogeochemistry: A Foundation for the Future*, Alsdorf, D., Tshimanga
1149 Muamba, R. Moukandi N’kaya, G.D., eds, AGU, John Wiley & Sons Inc.

1150 Peyrard, D., Sauvage, S., Vervier, P., Sanchez-Perez, J. M., & Quintard, M. (2008). A coupled
1151 vertically integrated model to describe lateral exchanges between surface and subsurface
1152 in large alluvial floodplains with a fully penetrating river. *Hydrological Processes*. 22,
1153 4257–4273 (2008) DOI: 10.1002/hyp.7035

1154 Prigent, C., Papa, F., Aires, F., Rossow, W. B., & Matthews, E. (2007). Global inundation
1155 dynamics inferred from multiple satellite observations, 1993-2000. *Journal of*
1156 *Geophysical Research Atmospheres*, 112(12), 1993–2000.

- 1157 <https://doi.org/10.1029/2006JD007847>
- 1158 Ramsar Convention on Wetlands. (2018). Global Wetland Outlook: State of the World's
1159 Wetlands and their Services to People. Ramsar Convention on Wetlands. (2018)., 88.
- 1160 Reggiani, P., Sivapalan, M., & Majid Hassanizadeh, S. (1998). A unifying framework for
1161 watershed thermodynamics: Balance equations for mass, momentum, energy and entropy,
1162 and the second law of thermodynamics. *Advances in Water Resources*, 22(4), 367–398.
1163 [https://doi.org/10.1016/S0309-1708\(98\)00012-8](https://doi.org/10.1016/S0309-1708(98)00012-8)
- 1164 Rosenqvist, Å., & Birkett, C. M. (2002). Evaluation of JERS-1 SAR mosaics for hydrological
1165 applications in the Congo river basin. *International Journal of Remote Sensing*, 23(7),
1166 1283–1302. <https://doi.org/10.1080/01431160110092902>
- 1167 Runge, J. (2007). The Congo River, Central Africa, in *Large Rivers: Geomorphology and*
1168 *Management*, edited by A. Gupta, chap. 14, pp.293–309. Wiley, U.K.
1169 <https://doi.org/10.1002/9780470723722.ch14>
- 1170 Runge, J., & Nguimalet, C. R. (2005). Physiogeographic features of the Oubangui catchment
1171 and environmental trends reflected in discharge and floods at Bangui 1911-1999, Central
1172 African Republic. *Geomorphology*, 70(3-4 SPEC. ISS.), 311–324.
1173 <https://doi.org/10.1016/j.geomorph.2005.02.010>
- 1174 Santos da Silva, J., Calmant, S., Seyler, F., Rotunno Filho, O. C., Cochonneau, G., & Mansur,
1175 W. J. (2010). Water levels in the Amazon basin derived from the ERS 2 and ENVISAT
1176 radar altimetry missions. *Remote Sensing of Environment*, 114(10), 2160–2181.
1177 <https://doi.org/10.1016/j.rse.2010.04.020>
- 1178 Sauvage, S., Sánchez-Pérez, J-M., Vervier, P., Naiman ,R-J., Alexandre, H., Bernard-Jannin,
1179 L., Boule^treau, S., Delmotte, S., Julien ,F., Peyrard, D., Sun, X., & Gerino, M. (2018).

1180 Modelling the role of riverbed compartments in the regulation of water quality as an
1181 ecological service. *Ecological Engineering*, 118:19–30.
1182 <https://doi.org/10.1016/j.ecoleng.2018.02.018>

1183 Schuol, J., & Abbaspour, K. C. (2007). Using monthly weather statistics to generate daily data
1184 in a SWAT model application to West Africa. *Ecological Modelling*, 201(3–4), 301–311.
1185 <https://doi.org/10.1016/j.ecolmodel.2006.09.028>

1186 Sloan, P.G., & Moore, I.D.(1984). Modeling subsurface stormflow on steeply sloping forested
1187 watersheds. *Water Resources Research*, 20, 1815–1822.

1188 Strauch, M., Bernhofer, C., Koide, S., Volk, M., Lorz, C., & Makeschin, F. (2012). Using
1189 precipitation data ensemble for uncertainty analysis in SWAT streamflow simulation.
1190 *Journal of Hydrology*, 414–415, 413–424. <https://doi.org/10.1016/j.jhydrol.2011.11.014>

1191 Strauch, M., & Volk, M. (2013). SWAT plant growth modification for improved modeling of
1192 perennial vegetation in the tropics. *Ecological Modelling*, 269, 98–112.
1193 <https://doi.org/10.1016/j.ecolmodel.2013.08.013>

1194 Sun, X., Bernard-Jannin, L., Garneau, C., Volk, M., Arnold, J. G., Srinivasan, R., Sauvage, S.,
1195 & Sánchez-Pérez, J. M. (2016). Improved simulation of river water and groundwater
1196 exchange in an alluvial plain using the SWAT model. *Hydrological Processes*, 30(2),
1197 187–202. <https://doi.org/10.1002/hyp.10575>

1198 Tourian, M., Tarpanelli, A., Elmi, O., Qin, T., Brocca, L., Moramarco, T., & Sneeuw, N.
1199 (2016). Spatiotemporal densification of river water level time series by multimission
1200 satellite altimetry. *Water Resources Research*, 52, 1140–1159.

1201 Tshimanga, R. M., & Hughes, D. A. (2011). Climate change and impacts on the hydrology of
1202 the Congo Basin: The case of the northern sub-basins of the Oubangui and Sangha Rivers,

- 1203 Physics and Chemistry of the Earth, 50-52,72–83, doi:10.1016/j.pce.2011.07.045.
- 1204 Tshimanga, R. M., Hughes, D. A., & Kapangaziwiri, E. (2012). Initial calibration of a semi-
1205 distributed rainfall runoff model for the Congo River basin. *Physics and Chemistry of the*
1206 *Earth*, 36(14–15), 761–774. <https://doi.org/10.1016/j.pce.2011.07.045>
- 1207 Tshimanga, R. M., & Hughes, D. A. (2014). Basin-scale performance of a semidistributed
1208 rainfall-runoff model for hydrological predictions and water resources assessment of large
1209 rivers: The Congo River. *Water Resources Research*, 50(2), 1174–1188.
1210 <https://doi.org/10.1002/2013WR014310>
- 1211 Tshitenge Mbuebue, J. M., Lukanda Mwamba, V., Tshimanga Muamba, R., Javaux, M., &
1212 Mahé, G. (2015). Wavelet analysis on the variability and the teleconnectivity of the
1213 rainfall of the Congo Basin for 1940–1999. International conference on the hydrology of
1214 African large river basins, FRIEND/ISI/IAHS, Hammamet, Tunisia, October, 26-30th.
- 1215 Van Griensven, A., Ndomba, P., Yalew, S., & Kilonzo, F. (2012). Critical review of SWAT
1216 applications in the upper Nile basin countries. *Hydrology and Earth System Sciences*,
1217 16(9), 3371–3381. <https://doi.org/10.5194/hess-16-3371-2012>
- 1218 Weng, P., Sánchez-Pérez, J. M., Sauvage, S., Vervier, P., & Giraud, F. (2003). Assessment of
1219 the quantitative and qualitative buffer function of an alluvial wetland: Hydrological
1220 modelling of a large floodplain (Garonne River, France). *Hydrological Processes*, 17(12),
1221 2375–2392. <https://doi.org/10.1002/hyp.1248>
- 1222 Werth, S., Güntner, A., Petrovic, S., & Schmidt, R. (2009). Integration of GRACE mass
1223 variations into a global hydrological model. *Earth and Planetary Science Letters*, 277(1–
1224 2), 166–173. <https://doi.org/10.1016/j.epsl.2008.10.021>
- 1225 Whittaker, G.; Confesor, R.; Di Luzio, M.; & Arnold, J.G.(2010). Detection of

1226 overparameterization and overfitting in an automatic calibration of SWAT. Transactions of
1227 ASABE 2010, 53, 1487–1499.

1228 Yuan, T., Lee, H., Jung, H. C., Aierken, A., Beighley, E., Alsdorf, D. E., Tshimanga, R.M., &
1229 Kim, D. (2017). Absolute water storages in the Congo River floodplains from integration
1230 of InSAR and satellite radar altimetry. *Remote Sensing of Environment*, 57–72.
1231 <https://doi.org/10.1016/j.rse.2017.09.003>

1232 Zhang, P., Liu, Y., Pan, Y., & Yu, Z. (2013). Land use pattern optimization based on CLUE-S
1233 and SWAT models for agricultural non-point source pollution control. *Remote Sensing*
1234 *of Environment*, 58(2), 230–244. <https://doi.org/10.1007/s12665-016-6058-7>

1235